NTNU – Trondheim
Norwegian University of
Science and Technology

Development of Test Methods for a Combined DC Power and Fiber Optic Deep Water Subsea Cable

Effect of DC Pre-stress on AC Withstand
Strength

Hans Kristian Hygen Meyer

Master of Energy and Environmental Engineering
Submission date: June 2015
Supervisor: Frank Mauseth, ELKRAFT
Co-supervisor: Sverre Hvidsten, SINTEF

Norwegian University of Science and Technology
Department of Electric Power Engineering

Problem Description

Repeatered Optical Cables (ROC) are used for fiber optic communication up to 10 000 km and down to 8 000 m depth. The cable consists of a conductor with integrated fiber optics, and the cable insulation is directly subjected to the sea water. The cable operates at 10 kV DC, supplying the repeaters needed to amplify the fiber optic signals. The ROC cable is also used for supplying power to subsea installations.

Currently there are no standards describing how to test such cables. The test methods should take relevant stresses, defects and service conditions into consideration.

The project work will mainly be experimental. The main purpose is to simulate possible defects in such a cable by using Rogowski-profiled test objects of the cable insulation with controlled metallic and organic contaminants and investigate the defects' effect on the cable lifetime. This will be done by applying a DC voltage equivalent to that of the current design test of the cable to the objects for various lengths of time, and AC step-up breakdown testing the objects afterwards. An analysis of the cable insulation raw material will also be undertaken to determine the nature of the contaminants that can end up in the extruded cable. A summer job at Nexans Norway, Oslo, is also offered in connection to the student project.

Preface

This thesis is part of an MSc in Energy and Environmental Engineering with a specialization in Electric Power Engineering at NTNU, carried out during the spring semester of 2015. The thesis was done in collaboration with Nexans Norway AS, with the purpose of developing test methods for Nexans Norway's combined fiber optic and DC power subsea deep water cable, ROC-2 (Repeatered Optical Cable 2), by investigating the AC and VLF strength of extruded HDPE insulation with various defects after DC pre-stressing. This thesis is a continuation of a project during the fall semester of 2014 at NTNU and Espen Sviland's master's thesis at NTNU during the spring semester of 2014.

Trondheim, June 18, 2015

Hans Kristian Hygen Meyer

Acknowledgment

I would like to thank the following people for their great help with this thesis:

Associate Professor Frank Mauseth, for being a very helpful and involved supervisor.

Co-supervisor at SINTEF Energy Research, Sverre Hvidsten, for giving good advice and assisting with the planning of the breakdown test program and raw material analysis.

Espen Sviland, for paving the way for this thesis with his project and master thesis, and the help and inspiration.

Hans Helmer Sæternes and Jorunn Hølto at SINTEF Energy Research and Pål Keim Olsen at NTNU, for the help with the laboratory work.

Jan-Are Sundby at Nexans Norway in Halden, for help with laboratory work at Nexans in Halden.

Finally, a thanks to Erlend Andersen and Bjart-Are Steinsland for staying engaged and everybody else at Nexans who has taken an interest.

<div align="right">H.K.M.</div>

Abstract

Repeatered fiber optic submarine cables require a very high reliability. The cables operate at a voltage of 10 kV DC to supply electrical power to the repeaters that are placed every 50-70 km along the cable to amplify the optical signal.

To ensure that the cable's polyethylene insulation system can operate without faults for 25 years, electrical test methods that take relevant stresses, defects and service conditions into consideration are needed. The ROC-2 cable is currently type-tested with 100 kV DC for 9 days under the assumption that an inverse power law relation holds for the insulation's electrical lifetime. Inverse power law relations are known experimentally to hold under AC voltage, but may not hold under DC.

Oxidized particles, metal inclusions and protrusions on the conductor are unavoidable in polymeric cables. An infrared spectroscopic analysis of 15 pellets with contaminants found in 23 kg of cable insulation raw material with a pellet scanner indicated the presence of oxidized material. Electrical degradation often occurs around such insulation irregularities, and they are thus a limiting factor in the insulation lifetime.

The long-term effect on the cable insulation of a DC field corresponding to an applied voltage of 100 kV DC over the cable was studied using Rogowski test objects with and without insulation irregularities in form of metal inclusions and oxidized particles.

The test objects were tested to breakdown with ramped 50 Hz AC voltage after different lengths of DC pre-stress (0, 9, 35 and 163 days). Some objects were breakdown tested with a ramped 0.1 Hz (VLF) before and after 35 days of DC pre-stress. In addition to this a few test objects were tested for partial discharge activity (PD) before and after 35 days of DC pre-stress.

No significant deterioration of the insulation was observed after the DC pre-stress. The AC breakdown strength of test objects without particles and test objects with oxidized particles seemed to increase after 163 days of DC pre-stress, but this is probably a result of manufacturing variations and statistical errors due to the small amount of test objects. The average VLF breakdown strength was at least 2-3 times as high as the AC breakdown strength.

PD inception in the insulation occurred at a lower field after 35 days of DC pre-stress, but the inception values are low enough to suspect surface discharges due to the conducting paint's poor adhesion to the insulation rather than internal discharges.

The results indicate that a long-term high DC field does not accelerate any of the tested breakdown processes in the cable insulation. The current type test's ability to detect the types of irregularities that have been found in the raw material and those that have previously been found in manufactured cable lengths is therefore questionable.

Sammendrag

Fiberoptiske sjøkabler må være veldig pålitelige. Kraft blir tilført kablene med 10 kV likespenning for å mate forsterkerenhetene som er plassert på kabelen med 50-70 km mellomrom for å forsterke det optiske signalet.

For å sikre at kabelen kan fungere feilfritt i minst 25 år trengs det elektriske testmetoder som tar høyde for relevante påkjenninger på og feil i polyetylen-isolasjonen. ROC-2-kabelen typetestes foreløpig med 100 kV DC i 9 dager under antagelsen om at isolasjonens elektriske levetid følger en invers potenslov. Det er kjent at inverse potenslover er gyldige under vekselspenning, men det er ikke like sikkert at dette er tilfellet under likespenning.

Oksiderte partikler, metallpartikler og ujevnheter på lederen er uunngåelige i polymeriske kabler. 15 pellets med indre forurensninger ble plukket ut fra 23 kg isolasjonsråmateriale med en pelletssjekker og disse ble funnet til å være oksidert polyetylen gjennom bruk av infrarød spektroskopi.

Langtidseffektene av et likespenningsfelt tilsvarende 100 kV likespenning over kabelen ble undersøkt ved å bruke Rogowski koppobjekter med og uten isolasjonsforurensninger i form av metallpartikler og oksiderte partikler.

Påvirkningen av DC-påkjenningen som funksjon av tid ble undersøkt ved hjelp av rampet 50 Hz holdfasthetstester der testobjektene ble tatt ut etter 9, 35 og 163 dager. Som referanse ble det utført holdfasthetstester på koppobjekter som ikke hadde vært utsatt for DC-påkjenning. Noen koppobjekter ble holdfasthetstestet med rampet 0.1 Hz (VLF) før og etter 35 dager med DC-påkjenning. I tillegg til dette ble noen få koppobjekter testet for partielle utladninger før og etter 35 dager med DC-påkjenning.

Ingen tydelig endring i isolasjonens AC-holdfasthet ble observert som følge av DC-påkjenningen. AC-holdfastheten til koppobjektene uten partikler og de med oksiderte partikler så ut til å ha økt etter 163 dager med DC-påkjenning, men dette er sannsynligvis et resultat av variasjoner i produksjonen og et begrenset antall testobjekter. Den gjennomsnittlige VLF-holdfastheten var minst 2-3 ganger så høy som AC-holdfastheten.

Isolasjonens PD-tennspenning så ut til å bli redusert av en 35-dagers DC-påkjenning, men svært lave tennspenninger tyder på at det kan være overflateutladninger som resultat av at sølvmalingen ikke festet seg godt nok til isolasjonen som er målt og ikke indre utladninger.

Resultatene tyder på at en DC-påkjenning over tid ikke akselererer noen av de testede feilmekanismene i kabelisolasjonen. På bakgrunn av forsøkene gjort i dette arbeidet er det derfor tvilsomt at den nåværende typetesten er i stand til å avdekke den typen feil som er funnet i råmaterialet og som tidligere er blitt funnet i ferdigprodusert kabel.

Contents

1   Introduction

1.1   Background

Fiber optic cables are essential to improve the growing communication networks be-
tween countries. One hair-thin optical fiber can transmit more than 10 terabits per
second, which is equivalent to 150 million telephone calls [1]. The cables also play
an important role in the control of subsea systems as the extraction of oil and gas is
moving from oil platforms to the sea floor.

The ROC-2 cable (see Figure 1.1 for cross-section) can be installed at 8000 m
depth and can stretch up to 10 000 km. At such large distances, the optical signal
must be amplified because of attenuation. The amplifiers in the ROC-2 cable are
placed every 50-70 km and fed using a DC voltage of up to 10 kV. To ensure that
the high density polyethylene (HDPE) insulation of the cable can withstand 10 kV
DC for a minimum of 25 years, the cable design has to be tested before the cable is
installed. This is called a type test. In addition to this, routine tests are performed
on all cable lengths to eliminate severe defects. The cable insulation system has to be
of very high quality as repairs of deep water subsea cables are very expensive. The
current type test for the ROC-2 cable is 100 kV DC for 9 days, but it has not yet been
proven that this test is equivalent to a service life of 25 years at 10 kV. Finding test
methods that take relevant stresses, defects and service conditions into consideration
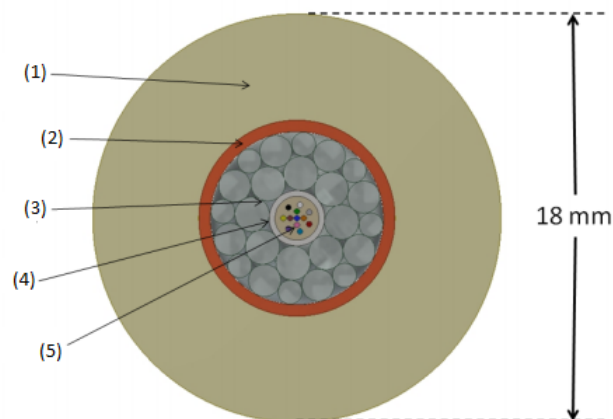for such cables is not straightforward.

Figure 1.1: Cross-section of the ROC-2 cable. (1) - HDPE insulation, (2) - Tubular copper
conductor, (3) - Armouring, (4) - Steel tube, (5) - Optical fibers. An inner copoly-
mer layer of 0.2 mm is not included in the figure. The thickness of the HDPE
insulation is 4.5 mm. [2]

1.2   Objectives

The main objectives of this project are to

1. Determine whether the field set up by a 100 kV DC voltage (10 times as large as the operating voltage) over the cable degrades the insulation significantly. 100 kV DC for 9 days is the current type test for the cable.

2. Determine the nature of the contaminants that can end up in the cable.

3. Propose possible modifications to the type test based on experiments and literature.

1.3   Approach

The effect of a strong DC field, equivalent to that of a 100 kV DC voltage over the cable, will be investigated by performing AC- and VLF-breakdown tests and partial discharge (PD) measurements on DC pre-stressed Rogowski-profiled test objects of the insulation material with various controlled defects (oxidized particles and metal particles) similar to the ones found by Sviland [2] in an ROC-2 cable sample. The DC pre-stress will be equivalent to that of the strongest field enhancement in the cable at 100 kV DC, and the test objects will be pre-stressed for various lengths of time before breakdown/PD testing to determine whether the AC/VLF-breakdown strength or PD-inception changes a function of time of pre-stress. The results will also indicate the effect of oxidized particles and metal inclusions on the breakdown strength and PD-inception after DC pre-stress. Results from the fall semester project (breakdown AC-step up tests after 0 and 9 days of pre-stress) by the author [3] are analysed alongside the results from the thesis work.

To determine the nature of the contaminants that can end up in the material, an analysis of the cable raw material will be performed, and the contaminants found will be analyzed further with FT-IR spectroscopy.

1.4   Limitations

The thesis will only allow testing a small number of samples. Therefore the results will only give an indication of what the true effects of the field and defects are on the material.

1.5   Structure of the Report

The rest of the thesis is organized as follows. In Section 2 some literature on properties and failure mechanisms of polyethylene insulation is presented together with

literature on test methods and infrared spectroscopy. Section 3 describes the experimental work, and Section 4 presents the results of the experiments. Finally, the results are discussed and conclusions are made in Sections 5 and 6. Parts of the fall semester project [3] are included in this thesis, but mostly in a modified and extended form.

2 Literature

2.1 Properties of Polyethylene Insulation

2.1.1 Structure of Polyethylene

Polyethylene is a polymer consisting of repeating monomer units of the hydrocarbon ethylene (C_2H_4). The chemical formula for polyethylene is $(C_2H_4)_nH_2$, where n, the degree of polymerisation, denotes the number of ethylene molecules in the polyethylene chain (typically in the range of $10^3 - 10^5$ [4]). The inter-molecular forces in polymer solids are of the secondary, van der Waals' type [4].

In practice, a polyethylene molecule is not a straight chain, but contains side branches of different lengths (see Figure 2.1). High density polyethylene (HDPE) has relatively few of such side branches, and can therefore be packed more closely than low (LDPE) and medium (MDPE) density polyethylene [5]. HDPE is therefore relatively hard and stiff compared to LDPE, MDPE and cross-linked polyethylene (XLPE), which makes it suitable for long-haul submarine cables as ROC-2, as the insulation's direct contact with the water and seabed makes it more vulnerable to surface damage.

Figure 2.1: Polyethylene chain with side branches [5, p. 9].

Polyethylene chains, consisting of up to tens of thousands of CH_2 groups, will in some areas run parallel to themselves and other chains, in what is called *crystalline* regions, while in *amorphous* regions, the chains will follow arbitrary paths. This is illustrated in Figure 2.2. Additives such as stabilizers and antioxidants are accumulated in the amorphous regions [6]. These are added to retard the inevitable deterioration of light- and oxygen-exposed PE, the effects of which are loss of strength, elongation and tear resistance [7].
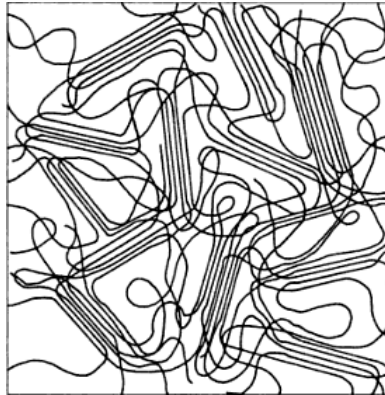
Figure 2.2: Long chains of polyethylene run parallell to each other through part of the volume before diverging, which gives rise to crystalline and amorphous regions [4, p. 12].

2.1.2 Electrical Properties of Polyethylene Insulation

Polyethylene has successfully been used as high voltage DC insulation for subsea communication cables since the 1950's [8]. As a result of advances in material technology and extrusion methods, polymer insulation has recently also been used for high-capacity HVDC transmission cables. Some of the advantages of extruded polymer insulation include higher conductor temperatures, easier jointing and lower maintenance costs [7, 9]. The electrical properties of polyethylene are outstandingly good, but XLPE is often preferred to conventional polyethylene as the former has a higher operating temperature, enabling it to carry larger current densities. The high intrinsic breakdown strength of polyethylene ($E \approx 500 kV/mm$) is hard to utilize in practice because the material has poor tracking resistance and degrades rapidly when there is partial discharge activity [7].

As the repair cost of submarine cables is roughly three times higher than for underground cables, the use of polymer insulation is more conservative for higher system voltages in submarine cables as it is difficult to detect weak points in extruded insulation [10].

A good insulator such as polyethylene is characterized by having a large band gap between what's known as the *conduction band* and the *valence band*. In the valence band, the electrons are strongly coupled to the atoms, while in the conduction band, the electrons easily leap from one atom to another. The energy levels of electrons are quantized, meaning that only a limited number of electron orbits are possible, all representing distinct energy levels - and the available orbits are concentrated in either the conduction band or the valence band. Because of this, there is a so-called *band gap* where there can be no electrons between the conduction and valence band which varies from material to material. Polyethylene has a wide band gap, meaning that the probability of electrons passing the gap is very small as the energy required

(usually expressed in electron volts, eV) is very high. The conductivity of a material can be expressed as [4]

$$\sigma = e \cdot n \cdot \mu \tag{2.1}$$

where e is the charge carrier ($1.6 \cdot 10^{-19}$ C for an electron), n is the concentration in numbers of carriers per cubic meter and μ is the mobility of the charge carriers, in velocity per kV/mm. The mobility μ varies over some decades, while the concentration σ varies with the band gap from ~ 0 (good insulators) to 10^{29} (good conductors). For polyethylene, only the amorphous regions contribute to the conductivity, the crystalline regions (see Figure 2.2) are in theory pure insulators with resistivity of at least 10^{20} Ωm. HDPE has a high degree of crystallinity (90 %) and therefore a resistivity of over 10^{18} Ωm, while LDPE (crystallinity of 55 %) has a resistivity of $\sim 10^{15}$ Ωm [6].

2.1.3 Mechanism of Oxidation

When exposed to air at elevated temperatures, polyethylene is susceptible to thermal oxidation. These changes in the material deteriorate its mechanical strength, flexibility and electrical breakdown strength [4], and change the conductivity - oxidation increases carrier mobility μ (see Equation 2.1) in LDPE but lowers it in HDPE [11, 12]. Polymer oxidation is a complex reaction that varies with the chemical structure of the polymer and the conditions at which oxidation occurs, but it is known that it is primarily in the amorphous regions of the polyethylene that oxidation takes place at lower temperatures [13]. According to Baum [14], the most important reactions in polyethylene oxidation are:

Initation:

$$\text{Formation of PE molecules with unpaired valence electrons (radicals) } R \cdot \tag{2.2}$$

Propagation:

$$R \cdot + O_2 \rightarrow ROO \cdot \tag{2.3}$$

$$ROO \cdot + RH \rightarrow ROOH + R \cdot \tag{2.4}$$

Termination:

$$2R \cdot \rightarrow R - R \tag{2.5}$$

$$R \cdot + ROO \cdot \rightarrow ROOR \tag{2.6}$$

$$2ROO \cdot \rightarrow ROOR + O_2 \tag{2.7}$$

In the initiation step (reaction 2.2), a radical $R\cdot$, in this case polyethylene molecules lacking a hydrogen atom $((C_2H_4)_nH)$, are formed by energy from sources such as radiation, heat or light [15].

In reaction 2.3, the hydrocarbon radical $R\cdot$ is reacting with oxygen, creating a new radical, $ROO\cdot$. This reaction happens readily after the reaction 2.2 has occurred [16]. $ROO\cdot$ then reacts with another polyethylene molecule RH (RH representing a polyethylene chain, $(C_2H_4)_nH_2$), forming $ROOH$ and another radical $R\cdot$ (reaction 2.4). The new radical then undergoes reaction 2.3 and reaction 2.4 leading to a chain reaction that can propagate hundreds of times before it is terminated [15].

The chain reaction can be terminated by coupling of radicals (reaction 2.5) or creation of inert products (reactions 2.6 and 2.7).

Antioxidants: Additives such as antioxidants are added in small portions to polymers, a typical polyethylene insulation material has one or two phenol (an aromatic group) antioxidants added to the extent of 800-1000 ppm [17]. Under some circumstances, antioxidants can aggregate into clusters of about 25 μm without ever being subjected to electric stresses, and local concentrations of antioxidants can be formed which promote oxidation instead of inhibiting it [4].

2.2 Electric Field Distributions

A perfect cable insulation material would be a homogeneous dielectric, with no electrical conductivity σ and a relative permittivity ϵ_r that's independent of temperature and voltage frequency. In such a material, the field distribution would be independent of the voltage shape [7].

All materials will however contain some free charge carriers in the form of ions or electrons, so the conductivity will never be zero. At 50 Hz AC, the losses due to conductivity will be relatively small compared to dielectric losses, but under DC, the field distribution will be determined by the conductivity.

This can be seen from the Maxwell law

$$\nabla \times \vec{H} = \vec{J} + \frac{\partial \vec{D}}{\partial t} \tag{2.8}$$

.

Taking the divergence of both sides and using Ohm's law $\vec{J} = \sigma \vec{E}$ and $\vec{D} = \epsilon \vec{E}$ gives

$$\nabla \cdot (\sigma \vec{E}) + \frac{\partial}{\partial t} \nabla \cdot (\epsilon \vec{E}) = 0 \tag{2.9}$$

In the phasor domain, Equation 2.8 becomes $\nabla \times H = J + j\omega D$, where H, J and D are phasors and ω is the frequency in rad/s. Taking the divergence of both sides and inserting Ohm's law $J = \sigma E$ and $D = \epsilon E$ gives

$$\nabla \cdot (\sigma E) + \nabla \cdot (j\omega \epsilon E) = 0 \tag{2.10}$$

If the frequency ω tends to zero (DC), Equation 2.10 tends to $\nabla \cdot (\sigma E) = 0$, whereas the higher ω is, the less important $\nabla \cdot (\sigma E)$ will be as the equation will be dominated by the $\nabla \cdot (j\omega \epsilon E)$ term (the fact that $\epsilon \gg \sigma$ for dielectrics also contributes to this). Therefore, ϵ is the parameter of interest at AC, while σ is the parameter of interest at DC. DC does however not occur in a pure form in reality, as the dielectric will be stressed in an AC manner when switched on or off [6]. AC and DC fields will be discussed in more detail below.

2.2.1 Field Distributions at AC

The flux density in an ideal dielectric is

$$\vec{D} = \epsilon \vec{E} \tag{2.11}$$

where $\epsilon = \epsilon_0 \epsilon_r$ is the permittivity and $\vec{E}$ is the E-field. The boundary condition $D_1 = D_2$ means that for two ideal dielectrics with permittivities ϵ_1 and ϵ_2 layered on top of one another, the field distribution is determined by the equation

$$E_1 = \frac{\epsilon_2}{\epsilon_1} E_2 \tag{2.12}$$

which means that the field will be highest in the material with the lowest permittivity, as is the case with an air bubble ($\epsilon_r = 1$) in polyethylene ($\epsilon_r = 2.3$). This resulting voltage distribution is called a *capacitive* voltage distribution.

2.2.2 Field Distributions at DC

A DC voltage will after a while produce a resistive field distribution, which is dependent on the conductivity of the materials. Ohm's law $J = \sigma E$ implies that the equipotential lines will be concentrated in areas with low conductivity σ. Therefore, the conductivity of the insulation, which increases with temperature and field strength, will be the parameter of interest for DC applications. At DC, Equation 2.9 tends to $\nabla \sigma E = 0$ as shown above, which means that for two dielectrics with conductivities σ_1 and σ_2 layered on top of one another, the field distribution is determined by the equation

$$E_1 = \frac{\sigma_2}{\sigma_1} E_2 \tag{2.13}$$

which is a *resistive* field distribution.

When connecting a DC-voltage, the voltage distribution will at first be capacitive, and a capacitive current

$$i_c = C \frac{dU}{dt} \tag{2.14}$$

will run. After the voltage has been switched on, a transient current called a polarisation current i_p runs which decreases slowly until a static leakage current is established. Charges are built up in the dielectric during this transition, creating layers of charges of either opposite or equal polarity to the adjacent electrode depending on the interface between the electrode and the dielectric. These layers of charge enhance the field in one area and decrease it in another [6].

If the electrode interface is not able to convey charges as fast as the dielectric conducts them, a layer of charges of opposite polarity will be formed at the electrode interface. These are called *hetero charges* (see Figure 2.3a), while the reverse situation gives rise to a layer of the same polarity as the electrode, *homo charges*. These charges get trapped in amorphous regions of the polymer and will therefore not vanish after the voltage has been switched off, and can remain for up to several days [6, 18]. The *depth* of the trap, defined as the energy needed to liberate the charge carrier from the trap, governs the time the charges stay trapped (a typical trap depth is about 0.8 eV [19]). Conduction in polymers is generally explained as hopping between such traps - the typical trap separation being about 2.8 nm, but the chemical and physical nature of the traps have not been explained [19].
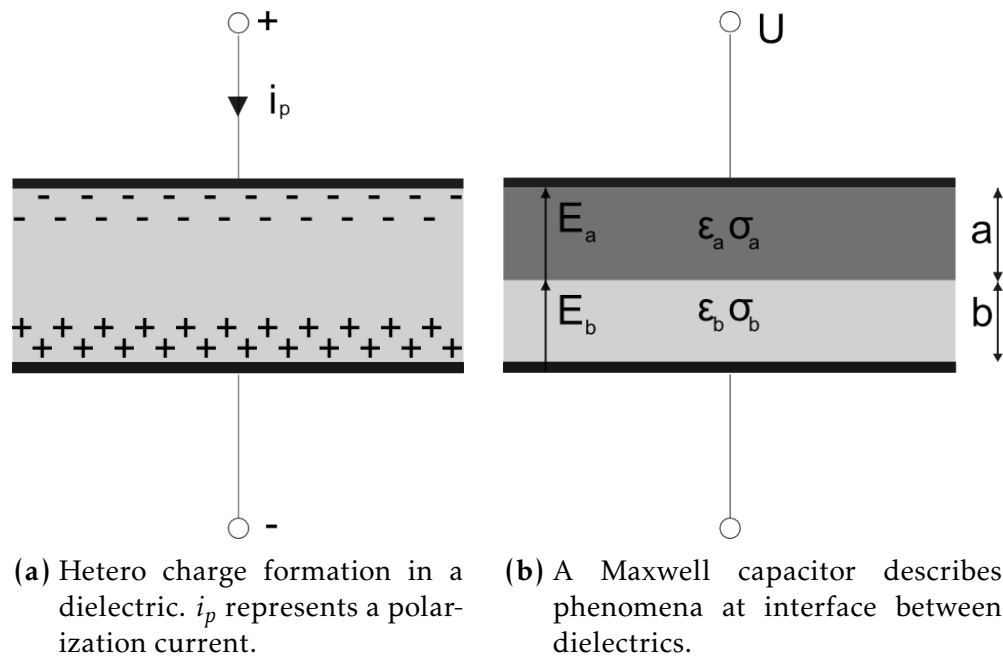

(a) Hetero charge formation in a dielectric. i_p represents a polarization current.

(b) A Maxwell capacitor describes phenomena at interface between dielectrics.

Figure 2.3: Heterocharges and Maxwell capacitor.

These situations have by Kreuger [6] been represented as an increased resistivity near the interface with the electrodes. The dielectric can then be treated as a combination of three dielectrics layered on top of each other, or a Maxwell capacitor with three layers (see Figure 2.3b for at two-layer Maxwell capacitor) with similar

permittivities but large differences in conductivity. Field calculations for a Maxwell capacitor are appended in Appendix C.

Surface charges will accumulate at interfaces between materials with different quotient ϵ/σ, such as in the case of a contaminant in cable insulation. The growth of these charges can be calculated with Gauss' law $\nabla \epsilon E = \rho$, however it is possible to calculate DC field distributions without resorting to surface charges [6], this is also shown in Appendix C.

Field stages of DC: As mentioned above, a "pure" DC field never occurs as a DC voltage always has to be switched on or off. Polarity reversals also give rise to special field phenomena. Kreuger [6] distinguishes the DC field into a total of seven stages, three of which are associated with polarity reversal, see Figures 2.4 and 2.5.

Stage I is the capacitive field, stage II an intermediate between the capacitive and resistive field, and stage III is the resistive field. Stage IV occurs after the voltage has been switched off, with surface charges on the interface between layers with different ϵ/σ remaining for some time until they disappear.

If the voltage polarity is suddenly reversed, a reversed capacitive field is imposed on the dielectric (stage V), which when superposed on the field induced from the layers of charge present in the dielectric can generate very high field strengths [6]. In stage VI, the field gradually changes to that of stage VII (the resistive field), forming new charges at interfaces between layers of different ϵ/σ.
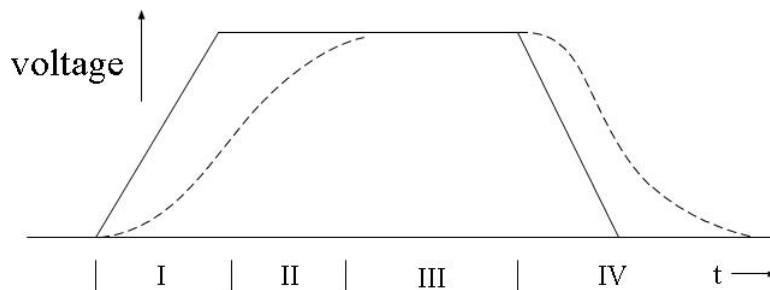

Figure 2.4: The different stages of DC when switching it on and off. The dotted line represents the growth and decline of internal charges, assuming that the rise- and switch-off time of the voltage is smaller than the time constant of the growth of internal charges [6].
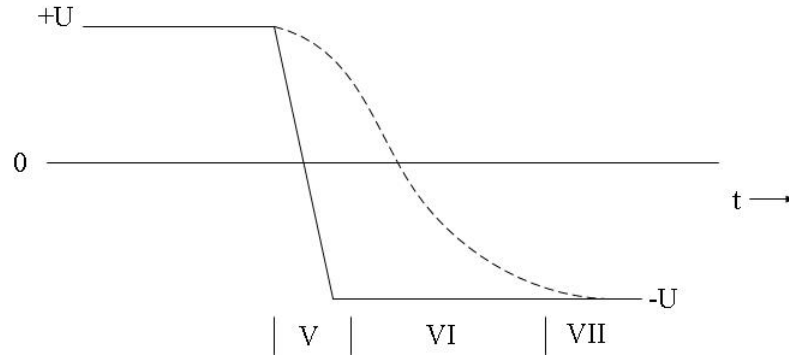
Figure 2.5: The different stages of DC in the case of a polarity reversal. The dotted line represents the growth and decline of internal charges [6].

The effect of temperature and field strength on conductivity: The conductivity of a material is highly dependent on temperature and field strength, whereas permittivity is not. This makes DC fields harder to calculate, as two more variables affect the fields than at AC. Temperature differences within the dielectric leads to local variations of the ratio ϵ/σ, which leads to layers of charges as discussed above.

At low fields polymeric dielectrics are generally ohmic as the energy gained by charge carriers between traps ($q\lambda E$, where q is the charge, λ the trap separation and E the field) is very low. At a certain field, for XLPE roughly 10 kV/mm, the energy gained between traps is comparable to the thermal energy which causes detrapping at lower fields - at this point the conductivity starts to increase with the field. At very high fields, when the energy gained between traps is comparable to the trap depth ($\approx$0.8 eV$\Rightarrow E = \frac{0.8eV}{q\lambda} = 285$ kV/mm), the material starts to look like a metal, although with a field limited to a fixed value different from zero [19].

The latter fields are normally restricted to regions in the μm range near stress enhancements with a very small radius of curvature such as a sharp protrusion. The field is called the space charge limited field (SCLF), as the field strength does not increase with applied voltage above the voltage at which the SCLF is reached [19]. As the mobility of the charge carriers is sharply increased in this situation, the insulation subjected to it acts like a resistor with relatively high conductivity, and space charges from a needle tip will be injected into the high field region until the field is reduced below the threshold of the SCLF [20].

2.3   Electrical Degradation of Polymer Insulation

Understanding the mechanisms that lead to failure of polymer insulated cables is important when developing design tests for such cables, as there may be different ageing processes at different stresses [7]. The better the failure mechanisms in the insulation are understood, the easier it is to devise relevant tests.

This section presents the most important causes of failure for polymer insulated cables.

2.3.1   Insulation Irregularities

Polymer insulated cables are manufactured in very clean conditions to avoid the inclusion of contaminants in the insulation. It is however impossible to completely prevent contaminants from entering the insulation, and these can reduce the lifetime or the short term AC or DC breakdown strength of the insulation [10, 21]. Gas-filled cavities are also hard to eliminate and can easily be formed during extrusion or moulding of the insulation material [7]. Dust particles entering the insulation can contain moisture or gas that can lead to void formation between the dielectric and the particles. Other processes that can create cavities are non-uniform contraction, mechanical stresses such as bending or slow chemical processes occurring after the manufacturing of the cable [7]. Such cavities may lead to partial discharges (PDs, see Section 2.3.3) if the electric field is high enough, which in turn can cause erosion of the material and ultimately electrical breakdown.

Contaminants in polymeric cable insulation are usually distinguished by whether they are *organic* or *inorganic*. Organic contaminants are typically oxidized insulation material, and can originate from the PE granules or be formed in stagnation zones in the extrusion line. There could be void formation around organic contaminants due to bad adhesion to the surrounding polymer [10]. Inorganic contaminants such as metal particles can originate from the granules, the extrusion equipment or the conductor, and can also be in the form of protrusions from the conductor.

Both types of contaminants are likely to have a different ϵ/σ than the surrounding polymer, leading to local field enhancements at DC.

28 irregularities of size 60-200 μm were found in 60 meters of ROC-2 cable by Sviland [2]. Of these, there were 21 voids, six oxidized particles and one metal particle.

2.3.2   Fast Voltage Changes at DC in the Presence of Defects

Research has shown that when a DC voltage is applied to a cable defect, space charges of the same polarity (homo charges) as the voltage will accumulate around the defect, and decrease with distance from it [22]. These charges will act as a shield around the defect, reducing the local field and thus making the DC withstand voltage of the defect artificially high, see Figure 2.6.
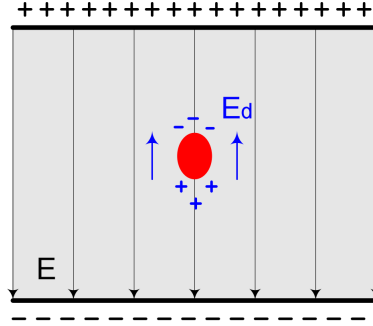
Figure 2.6: Space charge formation around a conducting defect, reducing the local field and making the DC withstand strength artificially high. Homo charges are built up around the defect [23].

As the charges are trapped and therefore can not change rapidly, they will in the case of a quick polarity reversal contribute to a local field enhancement that can be higher than the breakdown strength of the polymer. This is because the trapped homo charge becomes a hetero charge when the polarity is reversed. The field originating from the trapped charges will also lead to field enhancements during quick groundings and can be sufficiently strong to initiate treeing [24]. Generally, the redistribution of charges in a dielectric is given by the time constant [24]:

$$\tau_d = \frac{\epsilon_0 \epsilon_r}{\sigma(E, T)} \tag{2.15}$$

where $\epsilon_0 \epsilon_r$ is the permittivity and $\sigma(E, T)$ is the conductivity as a function of field strength and temperature. If the charge redistribution is to limit the electric field in the way explained above, τ_d in Equation 2.15 has to be comparable to the time constant for the change of the voltage, which is often not the case at AC.

Quick polarity reversals have in several studies been shown to be critical for extruded insulation [18]. A study on the effect of abrupt groundings on extruded cables found that the number of groundings needed to cause breakdown of a DC prestressed cable is dependent on the pre-stress voltage level and the steepness of the voltage wave created during grounding [25]. Other studies have found that XLPE insulation with a needle defect exposed to quick groundings after a DC pre-stress lead to electric tree initiation and ultimately breakdown [20, 23]. A quick grounding event in a cable will stress the areas close to where the grounding happened the most, as the impedance of the cable will reduce the rise time of the voltage impulse.

In [20], the effect of fast voltage rises on contaminants with different σ/ϵ ratio than the surrounding polymer is explained as a function of the conductivity of the polymer: the time constant for the redistribution of charge in dielectrics is generally given by Equation 2.15, where $\sigma(E, T)$ increases strongly with field and temperature, while $\epsilon_0 \epsilon_r$ remains constant. If the applied voltage varies with a time constant that's shorter than τ_d, the space charges are not allowed sufficient time to rearrange and

shield the defect, and the field around the sharpest tips will increase with the voltage, leading to charge injection into the high-field region if τ_d becomes low enough [20].

A needle at negative polarity (cathode) has been found to initiate local electrical breakdown at 20 to 40 times lower number of groundings than a needle at positive polarity (anode) [20]. This is explained as a higher space charge injection under the SCLF right outside the needle tip at negative polarity than at positive polarity, leading to a larger current density and higher heating when this charge is redistributed under a grounding [20].

A conductive particle that's embedded in the insulation will become polarized, and the particle will have both an anode and a cathode type of interface with the surrounding dielectric. In the case of a quick grounding, anode and cathode effects should occur simultaneously, and cathode effects will likely be more severe for the reasons mentioned above. Test objects with embedded needles have been shown to withstand a higher number of groundings than test object with needles in contact with the cathode, which is likely due to a more limited capacity for injection of space charges for the embedded needle [20].

2.3.3 Partial Discharges

A partial discharge (PD) is a breakdown of only a part of the dielectric. It occurs in gas-filled cavities at both AC and DC, and can slowly erode the material [6, 26]. The PD-induced degradation is a result of chemical degradation and bombardment of particles (nitrogen ions) [27]. Spherical cavities of different sizes can be present in moulded insulation [7]. Partial discharges can occur in such cavities if the field strength in the cavity exceeds the dielectric strength of the gas in the cavity, which is given by the Paschen curve for that gas (~ 3 kV/mm for the largest air-filled voids at atmospheric pressure [4]). Figure 2.7 shows a modified version of the Paschen curve for air, where the field strength instead of voltage at breakdown is plotted.
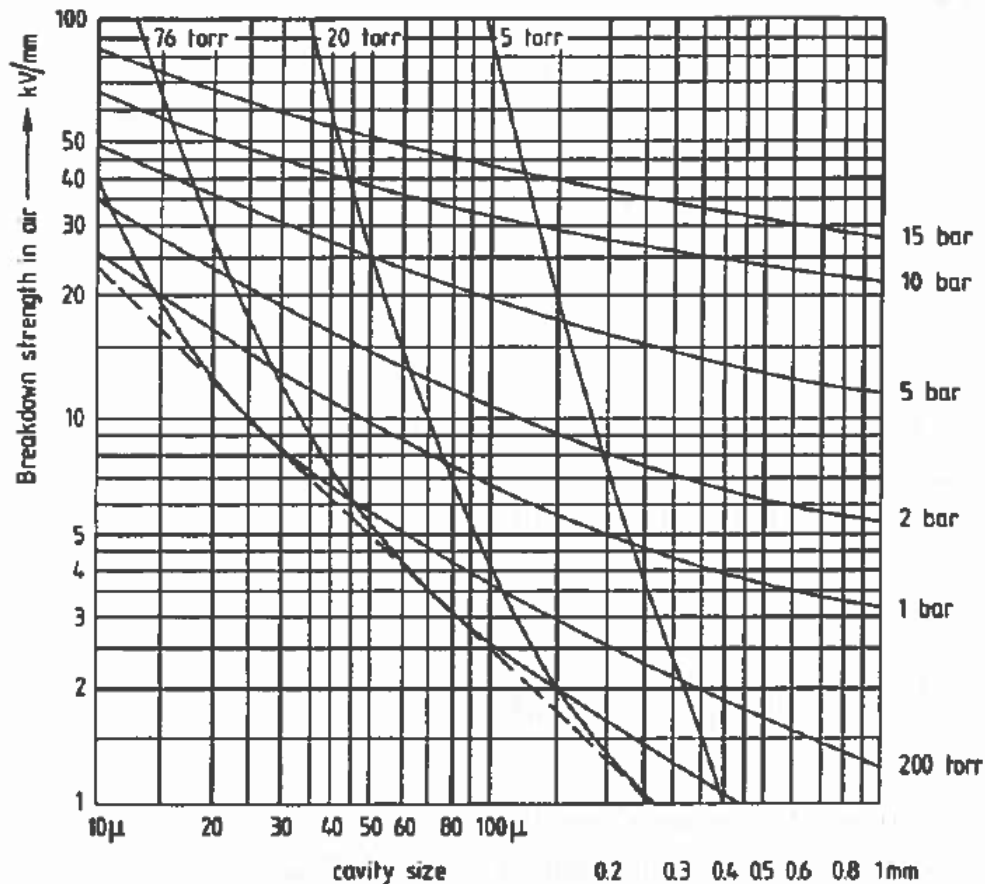
Figure 2.7: Modified Paschen's curve, with field strength at breakdown in air as a function of cavity thickness and air pressure. The straight dotted line is the minimum of the Paschen curve - if the pressure in the cavities is not known, one has to stay under this line to avoid partial discharges [28].

The interaction between the PD in a cavity and the surrounding dielectric is complex as the PD activity changes the dielectric (aging), at the same time as the PD mechanism is affected by that very aging [27].

Partial discharges can also occur on surfaces (surface discharges) or they can be in the form of corona. Internal discharges are the most relevant type in this work.

PDs at AC: An equivalent circuit for a cavity in a dielectric called the abc model (see Figure 2.8) is valid for AC fields and the capacitive stage of DC fields. The voltage over the cavity in the abc model in the case of AC is shown in Figure 2.9 [29]. The AC voltage applied, V_a, leads to begin with to a voltage over the cavity of $V_c = \frac{C_b}{C_b+C_c} V_a$ (V_c and V_a in RMS-values). When the voltage over the cavity reaches the ignition or start voltage $U^\pm$ of the cavity (follows from the Paschen curve of the gas

in the cavity), a discharge occurs, leading the voltage to drop to a residual voltage $V^{\pm}$. The discharge is extinguished immediately and therefore the voltage over the cavity is again increased as if the discharge had not occurred, but now it is offset by $\Delta V = U - V$.

As the voltage is increased, the breakdown voltage $U^{\pm}$ is again reached and the process is repeated, leading to a recurrent discharge pattern as the one shown in Figure 2.9. Discharge patterns can reveal whether the origin of the discharges are internal, surface or corona. Internal and surface discharges will have discharge patterns like the one in Figure 2.9 (discharges right before the voltage peak), while corona will typically discharge around the negative polarity peak of the voltage.

If the applied voltage is adjusted so that a discharge occurs every time the voltage reaches its peak value, it can be shown that the number of discharges n per half-cycle is [7]

$$n = \frac{2(\frac{C_b}{C_b+C_c}\sqrt{2} - V)}{U - V} \tag{2.16}$$

Partial discharge measurements are usually made by increasing the voltage in steps until a voltage level where PDs are observed is reached, called the *inception* voltage U_i, and then lowering the voltage until they disappear, that voltage level is called the *extinction* voltage U_e (both in RMS values). Inception U_i occurs when the peak value of the voltage over the void V_c is equal to the ignition voltage of the cavity [7]

$$U = \frac{C_b}{C_b + C_c}\sqrt{2}U_i \Rightarrow U_i = \frac{C_b + C_c}{C_b}\frac{U}{\sqrt{2}} \tag{2.17}$$

An expression for the extinction voltage is found by setting $n = 1$ in Equation 2.16, as there will by just one discharge each time the voltage reaches its peak value just above the extinction voltage. The expression for U_e becomes [7]

$$U_e = \frac{C_b + C_c}{C_b}\frac{U + V}{2\sqrt{2}} \tag{2.18}$$

which is $U_e \approx \frac{1}{2}U_i$ if $V \ll U$. This approximation is the lower limit for the extinction voltage U_e.
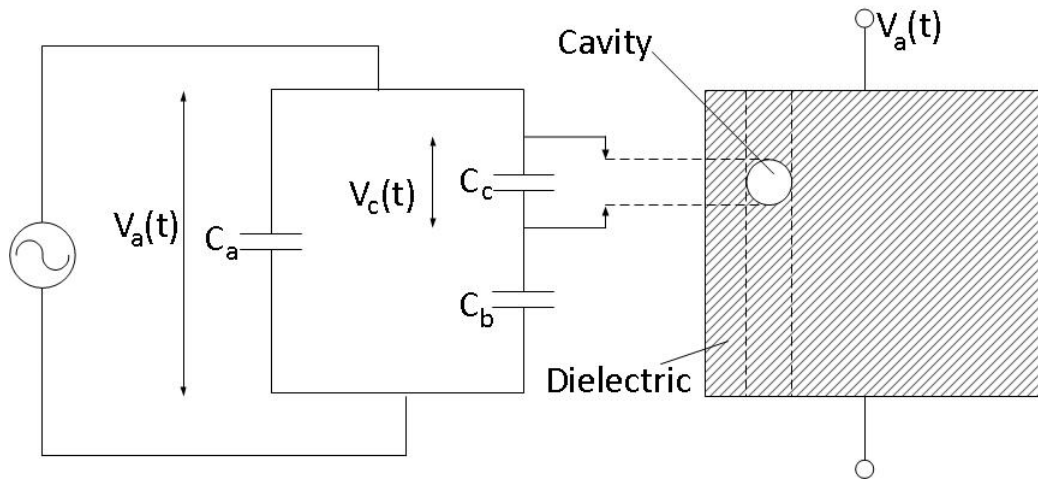
Figure 2.8: The abc model. C_c is the capacitance of a cavity in the dielectric, while C_b is the capacitance in series with the cavity and C_a represents the capacitance of the rest of the dielectric. $V_a(t)$ is the voltage applied to the dielectric and $V_c(t)$ is the voltage over the cavity.
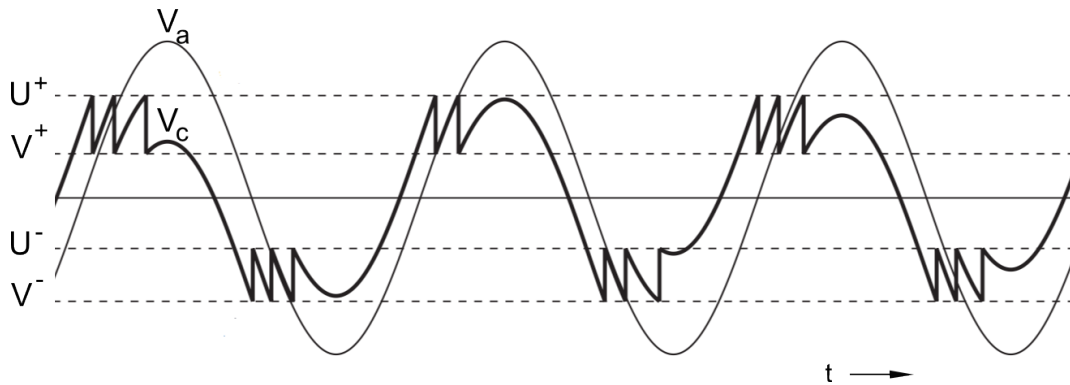

Figure 2.9: Illustration of partial discharges in a cavity during AC, calculated from the abc model. A discharge occurs in the cavity when the breakdown voltage of the cavity $U^\pm$ is reached, and the voltage V_c over the cavity drops until the residual voltage $V^\pm$ is reached, leaving the gap partially discharged. V_a is the applied voltage [29].

Different types of void geometries will lead to different field enhancements at AC. A fissure parallel to the electrodes or a fissure between an electrode and an insulation with relative permittivity ϵ_r leads to a field in the cavity that's ϵ_r times higher than the field E_d in the surrounding insulation, while a fissure in the direction of the field has a field that's equal to that of the surrounding field. A spherical void has a field strength of [28]

$$\frac{3\epsilon_r}{1 + 2\epsilon_r} E_d \qquad (2.19)$$

PDs at capacitive stage of DC: Discharges during the capacitive stage of DC bear resemblance to the discharges at AC. The abc model in Figure 2.8 holds. The discharge intensity n is approximated as being proportional to the steepness $\frac{dV_a}{dt}$ of the applied voltage and to the ratio C_b/C_c and inverse proportional to the breakdown voltage U of the cavity [6].

PDs at resistive stage of DC: The abc model in Figure 2.8 must be adjusted when the DC field enters its resistive stage by adding leakage resistances R_a, R_b and R_c in parallel with C_a, C_b and C_c respectively. This leads to a voltage growth over the cavity [6]

$$v_c(t) = \frac{R_c}{R_b + R_c}(1 - e^{-t/\tau})V_a \tag{2.20}$$

where the time constant $\tau = \frac{R_b R_c}{R_b + R_c}(C_b + C_c)$. When $v_c(t)$ reaches the breakdown voltage V_i of the cavity, a discharge takes place. This process is repeated, with the time between two discharges, the recovery time t_r, being [6]:

$$t_r = -\tau ln(1 - \frac{U}{V_s}) \tag{2.21}$$

where $V_s = \frac{R_c}{R_b + R_c}V_a$ is the voltage the cavity would eventually reach if there was no breakdown in the cavity.

Setting $U = V_s$ in Equation 2.21 means that the recovery time t_r will tend to ∞. It is therefore much more difficult to find an inception voltage at resistive DC than at AC, as discharges at 50 Hz AC occur at least 50 times per second, while one could wait indefinitely from one discharge to the next at resistive DC.

PDs at the intermediate stage of DC: The discharge frequency during stage II in Figure 2.4 will follow the polarization current which gradually becomes the leakage current of stage III. Therefore the discharge frequency is time-dependent with a time constant that depends on the insulation material [6].

In reality, there will however be a time delay that's not constant after the breakdown voltage U of the cavity is reached as a starting electron needs to appear [6].

Measuring PDs Both non-electrical and electrical PD measurements are performed in the same way at AC and DC. The focus in this work will be on electrical PD measurements.

The displacement of charge occurring in the cavity in the abc model (see Figure 2.8) in the case of a discharge can be expressed as $q \approx \Delta V(C_b + C_c)$ where $\Delta V = U - V$ is the voltage drop over the cavity [7]. This charge cannot be measured in the external circuit, but a small voltage drop ΔU over C_a can be observed. A transient current

in the external circuit will restore the voltage across the test object, representing an *apparent charge* q_a. The apparent charge is proportional to the discharge energy in the cavity and can be used to measure the discharge magnitude by using a measuring impedance Z_m and a coupling capacitor C_k in a so-called straight detection circuit [7].

The coupling capacitance C_k is placed in parallel with the test object to form a high frequency path for the discharge current. C_k delivers a current pulse that's proportional to the apparent charge q_a each time a discharge takes place in the test object to compensate for the voltage drop, and this pulse is measured over the measuring impedance Z_m, which can be placed in series with C_k or in series with the test object [7]. C_k should be larger than C_a so that most of the current will be supplied in the external circuit. The circuit is calibrated by injecting a known charge magnitude over the test object.

See Figure 3.7 in Section 3.7 for a diagram of a PD measuring circuit.

2.4   Breakdown Mechanisms of Polymer Insulation

The physical reasons of electrical breakdown of solid dielectrics can be classified into three categories [7]:

1. *Intrinsic breakdown* of solids occurs only in pure materials of small volumes, without any inclusions, impurities, cavities etc. It occurs when the stress is high enough to make the dielectric conducting by creating a large amount of free electrons in the dielectric that quickly scatter and cause breakdown (these electrons have leaped from the valence band to the conduction band, see Section 2.1.2). In practice, insulating materials break down at much lower levels than the intrinsic breakdown strength.

2. *Thermal breakdown* occurs when there is excessive heating of the material caused by dielectric losses (AC) or conductivity losses (DC) [28]. Thermal breakdown is independent of the insulation thickness, but depends on the cooling of the cable. The thermal breakdown voltage for polyethylene is in the range of 3-5 MV at AC [7]. In the case of DC, the thermal breakdown is far higher than that of AC, and it is never reached in practice [28].

3. *Breakdown due to electrical degradation of the insulation* such as electrical treeing or water treeing. The final breakdown in this case could happen by mechanisms 1. or 2.

2.4.1   Partial Discharges and Electrical Tree Growth

Partial discharges are the main cause of breakdown at AC [28] but their occurrence is much rarer in the case of DC (see Section 2.3.3). Partial discharges cause erosion

on the wall of the cavities in the dielectric, creating pits that grow to one or more tubular channels of ~1-10 μm in diameter, forming a tree-like structure. Early theories explained this as an increase of the field strength at the tip of the pit causing intrinsic local breakdown, but recently it has been demonstrated that an injection of space charges that takes place above a certain local field stress could be important during tree inception. Some of these charges end up in deep traps that will cause field enhancement at voltage reversal (similar to the process that's described in Section 2.3.2), the result being a region of degraded insulation at the tip of the tree [7]. The aging process due to PDs that results in the treeing mechanism discussed above and ultimately breakdown can be summarized as [27]

1. The conductivity of the surface of the cavity increases due to PD-induced reaction processes with the air.

2. The surface roughness increases due to particle bombardment and deposition of PD by-products.

3. Localized crystals of PD by-products are formed.

4. The field enhancement at the crystal tips intensifies the local PD activity, causing pit formation.

5. Tree growth, possibly breakdown.

2.4.2 Effect of Field Strength on Voltage Life

AC: The effect of field strength E on voltage life L has for AC been determined experimentally as [28]

$$L = \frac{c}{E^n} \tag{2.22}$$

where c and n are constants. Equation 2.22 can therefore be used to predict the life of AC applications by using accelerated testing and extrapolation. This is usually done by a combination of step-up (ramped) breakdown tests and constant stress breakdown tests at different voltage levels, where the voltage and time of the breakdown is noted, and a life exponent n estimated. Ramped breakdown tests are preferred as the constant stress tests are time consuming. For polyethylene, the value of the life exponent n has been found to be in the range of 8-14 at AC [7], which means that the field strength has a great impact on the voltage life (a doubling of the field strength causes in the worst case a $2^{14} \approx 16000$ times shorter voltage life).

DC: Occurrence of partial discharges and treeing are far rarer at DC voltage [30]. Therefore, the D.C. design stresses may be 2-3 times as high as AC design stresses [28]. The operating conditions, such as the occurrence of rapid groundings, polarity

reversals or voltage spikes in combination with stress enhancements due to defects are very important for the voltage life of DC applications.

Some efforts have been made to find the value of the life exponent *n* for DC-operated telecommunication cables. Chen and Davies [31] found a DC life exponent *n* of Rogowski-profiled LDPE insulation objects of 9.97, 8.97 and 9.42 for objects without inclusions, with metallic inclusions, and with 50 *µ*m cylindrical voids respectively. Dissado et al. [32] also interpreted findings with an inverse power law, finding a life exponent *n* of 6.9 and 11.6 for two different joint mouldings (typical "weak links" in a cable due to regions of amalgamations) for DC-operated submarine telecommunications cables. See the next section for more on the difficulty of predicting the voltage life of DC applications as compared with AC.

2.5 Methods for Testing Extruded Polymer Insulated DC Cables

2.5.1 Routine Tests and Type Tests

There are two types of high voltage tests for the ROC-2 cable; a routine test and a type test. The routine test for DC-operated submarine telecommunications cables is usually in the range of 30-50 kV DC for ~5 min and is performed on all cable lengths to eliminate serious manufacturing defects that could cause system failures within months of operation [32].

Detecting dangerous particles in HVDC cables can be done with HVAC, but the critical flaws at HVAC may not be the same as at HVDC. PDs in voids might not be as detrimental at DC as AC as the PD rate at DC is much lower [25].

Another possibility could be very low frequency (VLF) testing at 0.1 Hz or rapid groundings at DC [23]. 0.1 Hz VLF has been found to require 2-3 times as high voltage as AC to eliminate the same defects in a comparable time [30]. Gnerlich [22] found that VLF testing works well for cables with few but large defects as the VLF test faults the defects with minimal damage to the rest of the cable. The VLF testing equipment is more convenient than the equivalent HVAC equipment when testing long cables, as the lower frequency reduces the apparent power needed.

As a routine test, every length of the ROC-2 cable is tested at 40 kV DC for 10 minutes. The type test, on the other hand, is only performed once on the cable, with the aim of proving that the cable can endure 10 kV for 25 years. The current type test for the ROC-2 is 100 kV for 9 days.

2.5.2 Life Estimation

Organic insulating materials will experience a decrease in breakdown voltage with time because of a gradual deterioration of the material due to electrical stress, mechanical stress, temperature and environmental factors such as moisture and pollution [7]. In the case of DC-cables such as the ROC-2, operating stresses such as rapid

groundings or polarity reversals will have a detrimental effect on the DC breakdown strength of the insulation [23, 30].

The lifetime of cables such as the ROC-2 is therefore limited, and it is necessary to know what level of stress the cable can withstand for the service life of 25 years.

As it is not feasible to conduct tests for 25 years before putting electrical power equipment into service, accelerated life tests are used to determine the lifetime of the equipment. Accelerated life tests are tests where the stresses are increased beyond what is assumed to be operating conditions. The life of the equipment is usually defined as the time to breakdown when electric stress is involved in the test [7].

The standard ITU-T G.976, clause 8.2.4.3, recommends the following test procedure for testing optical fibre submarine cable systems:

> **Test method:** A long cable is placed in a pool filled with conductive water at ground potential. A positive DC voltage is applied between the metallic conductor of the cable and water. No voltage breakdown must occur before the requirements of the reliability model are met.

> **Test conditions:** The voltage applied follows the formula VT^k where V is the service voltage, T is the test duration and k is a constant. The values of V and T selected for the test are based on the reliability model for cable and joints, taking into account the electrical loading that they will need to endure during their design lifetime. The acceleration factor k is empirically determined, and is specific to the insulation material used.

This standard describes a test method based on a power law relation between voltage life and field strength similar to the inverse power law in Equation 2.22. This relation has been shown experimentally to be correct at AC, and can be used to predict the AC life time of the insulation if the following assumptions and conditions are satisfied [31]:

1. The degradation and failure mechanisms are the same for constant and ramp tests

2. Constant stress tests are performed at the breakdown stress value from the ramp test

3. The distribution failure probability is the same for constant and ramp tests

The assumptions may not hold under DC voltage as the effect of the ramp rate is complicated by charge injection and trapping and therefore do not contain sufficient information to determine the statistics of breakdown [4, 31]. The approach does not take into consideration the time-dependence of the effective stress E_{eff} on the insulation under DC, which in practice is determined as [33]:

$$E_{eff} = E_a + E_s \tag{2.23}$$

where E_a is the applied field E_s is the component of the E-field originating from space charge distributions.

If it is assumed that Equation 2.22 with n from 6.9 to 11.6 (see Section 2.4.2) is relevant for the ROC-2 cable, the estimated lifetime at 10 kV $t_2 = t_1 \cdot (\frac{U_1}{U_2})^n$ for a cable that can withstand 100 kV for 9 days becomes much higher than 25 years.

2.6   Infrared Spectroscopy

Infrared spectroscopy can be used to e.g. determine the degree of oxidation of samples of polymer insulation material by exposing the samples to a range of IR electromagnetic radiation and recording the absorption spectra. IR spectroscopy involves measuring the absorption by the sample in the region from wavenumbers 4000-600 cm^{-1}, i.e. wavelengths of 2.5-16 μm.

2.6.1   Molecular Level

The energy of a molecule consists partly of translational energy, partly of rotational energy, partly of vibrational energy and partly of electronic energy, and the vibrational energy gives rise to absorption bands throughout most of the infrared region of the electromagnetic spectrum as the infrared radiation is absorbed and converted into energy in the form of molecular vibration. Every bond in a molecule vibrates, changing its dipole moment, and this change in dipole moment provides a mechanism for the absorption of radiation.

Every bond in a molecule has a characteristic absorption peak in the IR spectrum and thus the nature of a substance can be determined by comparing its IR absorption spectrum to that of a known sample. Functional groups such as O-H, C-H, C=O or C=C have characteristic narrow absorption frequencies in the IR spectrum and their presence in a sample can therefore be identified (see Table 2.1) [34, 35].

Table 2.1: Infrared absorption frequencies of common functional groups [34]

Functional group	Absorption range $[\text{cm}^{-1}]$
N-H	3500-3250
CON-H	3500-3000
O-H	3700-3200
COO-H	3200-2200
C-H	3100-2700
C≡N	2300-2200
C≡C	2250-2100
C=O	1850-1640
C=C	1680-1590
Aromatic	1600-1500

The absorption of infrared radiation is quantized, meaning that energy is absorbed only at certain frequencies, which would in theory give rise to a spectrum of discrete lines. However, the infrared spectra occur as bands rather than as lines since a change in vibrational energy is accompanied by a number of rotational energy changes.

Molecules vibrate by either stretching or bending. The former is a rhythmical movement along the bond axis, decreasing and increasing the distance between the atoms, while the latter can be a change of bond angle between bonds with a common atom or a movement of a group of atoms with respect to the remainder of the molecule without movement of the atoms in the group with respect to eachother [36].

Each atom in a molecule has three degrees of freedom, since they exist in a three-dimensional space. This means that a molecule of n atoms has $3n$ degrees of freedom. Removing the three degrees of freedom of translational and the three degrees of freedom of rotational motion leaves $3n$-6 vibrational degrees of freedom, also called fundamental vibrations. Thus large molecules such as polyethylene chains have many fundamental vibrations. The methyl groups (CH_2) in polyethylene have six fundamental vibrations (the $3n$-6 rule does not apply as the group only represents part of a molecule). See Figure 2.10 and Table 2.2 for details about the methyl groups' vibrational modes.
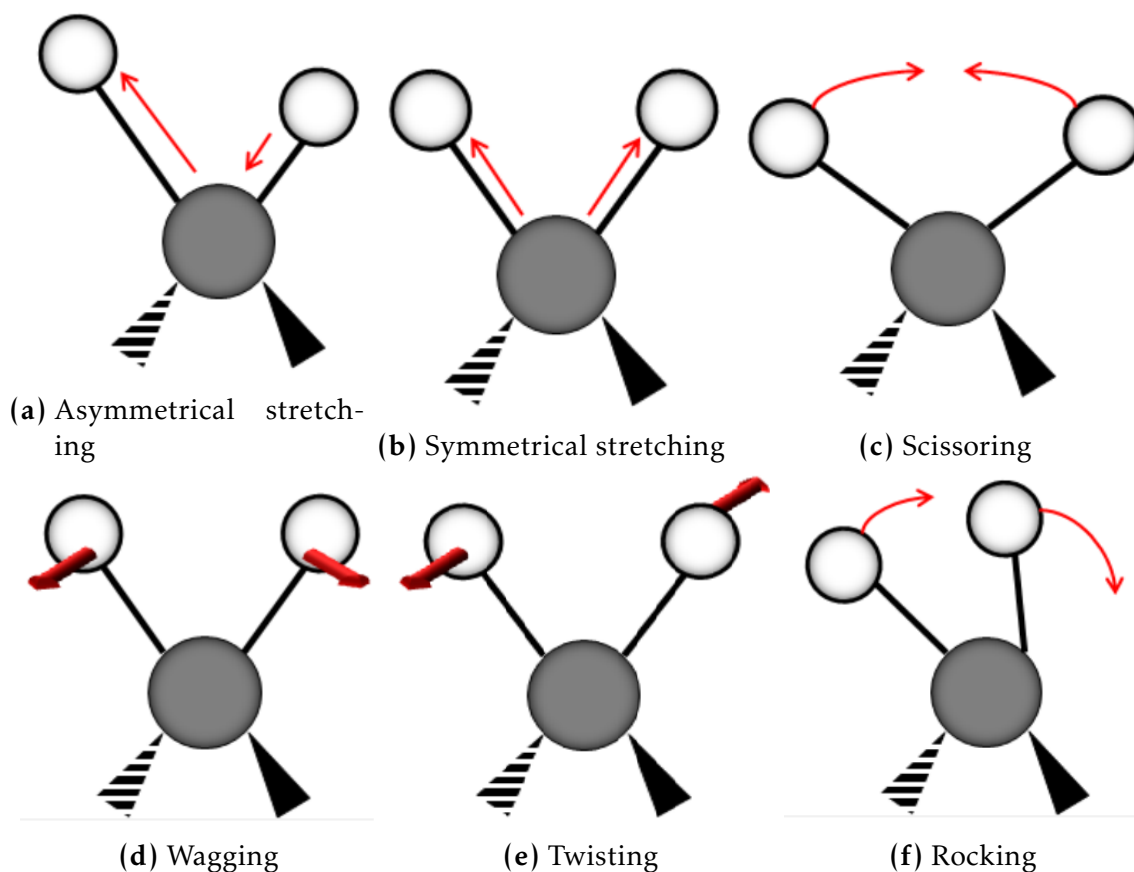
(a) Asymmetrical stretching

(b) Symmetrical stretching

(c) Scissoring

(d) Wagging

(e) Twisting

(f) Rocking

Figure 2.10: Vibrational modes for a CH_2 group [2].

Table 2.2: Infrared absorption frequencies of methyl vibrational modes [36].

Vibrational mode	Absorption range $[cm^{-1}]$
Asymmetrical stretching	~2926
Symmetrical stretching	~2853
Scissoring	1465
Wagging	1350-1150
Twisting	1350-1150
Rocking	~720

2.6.2 The Carbonyl Group: C=O

The carbonyl group is present in many different classes of compounds, such as aldehydes, ketones, carboxylic acid and esters (see Figure 2.11). Carbonyl groups are easily formed by the process of oxidative chain scission and other reactions that have been described by Hölmström and Sörvik in [37] after the oxidation reactions described in Section 2.1.3 have taken place. The carbonyl group band in the IR spec-

trum is easy to identify as it has a strong absorption band due to the C=O stretching vibration and because it occurs in a relatively interference-free region [38].

The oxidation of PE thus leads to a continuous broadening of the carbonyl band (1850-1550 cm^{-1}, see Table 2.3) in the IR spectrum at all temperature levels due to the increased relative amount of carbonyl groups.
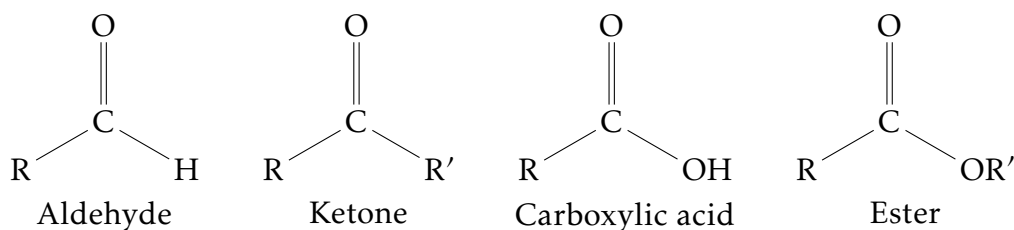
Figure 2.11: Some carbonyl compounds. R and R' are hydrocarbon chains.

Table 2.3: Infrared absorption frequencies of some important carbonyl groups [34]

Functional group	Absorption range [cm^{-1}]
Ester	1755-1730
Aldehyde	1740-1715
Ketone	1725-1700
Carboxylic acid	1725-1700

2.6.3 Beer-Lambert's Law

The spectra are expressed as transmittance (T), often as percentage values (%T) as compared with the spectrum of the background transmittance (the air, glass and other things the IR beam hits that's not the sample) or absorbance (A). Transmittance is the ratio of the radiant power or intensity (usually in watts) transmitted by a sample (I) to the radiant power that the sample is subjected to (I_0). If a sample has a thickness d, and a concentration c, the equation governing the absorption of radiation as function of transmittance is

$$T = \frac{I}{I_0} = 10^{-\alpha cd} \tag{2.24}$$

where α is called absorptivity and is dependent on the material and the frequency [35]. Equation 2.24 can be written as $log_{10}(I/I_0) = \alpha cd$, and the term $log_{10}(I_0/I)$ is called absorbance. So absorbance $A = \alpha cd$, and this is known as Beer-Lambert's law (see Figure 2.12).
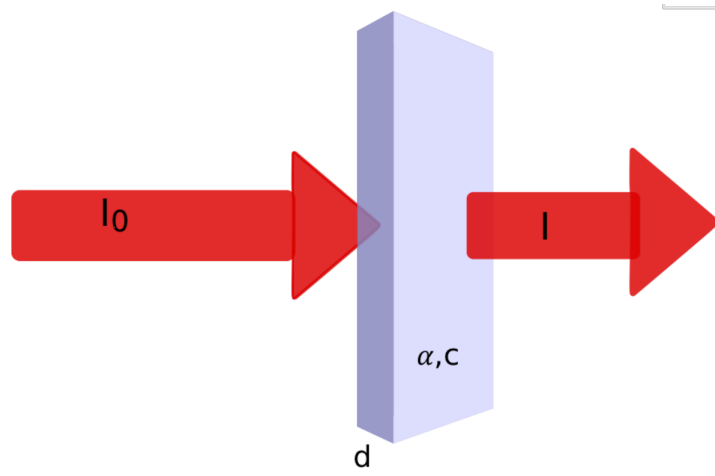
Figure 2.12: Illustration of Beer-Lambert absorption [39]

3 Method

3.1 Extruding

The HDPE insulation material is delivered as granules. Moulding test objects directly from PE granules risk creation of internal interfaces and entrapment of particles in the objects because of the large surface area of the granules. Such irregularities in the moulded objects will weaken the insulation and could be a source of error. Therefore, the granules are melted and mixed by the extruder to tape and film, which are more convenient for moulding. The extruder used was a Collin E20P. A schematic of the extruder is shown in Figure 3.1, and the process temperatures of the zones specified in Figure 3.1 are presented in Table 3.1.
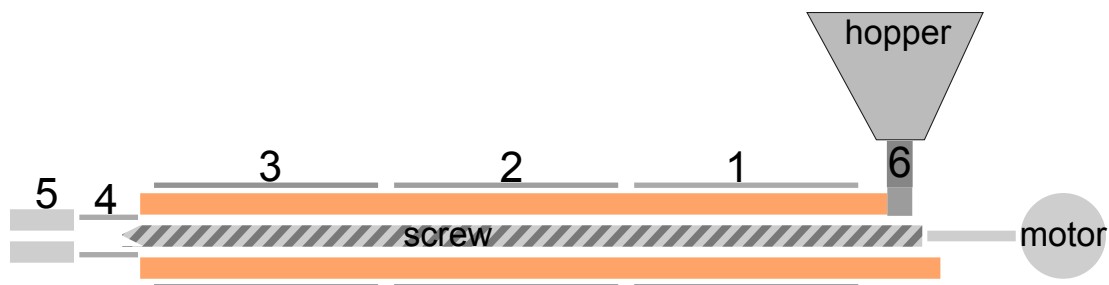
Figure 3.1: Schematic of the extruder. 1-6 are heat zones, see Table 3.1 for settings. The temperature in zone 6 was kept around ambient 20 °C with cooling water to avoid condensation. Temperature zone 5 is the temperature of the die.

Table 3.1: Zone temperatures of the extruder

Zone	1	2	3	4	5
T [°C]	160	180	200	190	190

3.1.1 Film

Firstly, granules were extruded to a thin film by using a die with 0.5 mm x 100 mm opening. The film was passed over two metal drums cooling it before rolling it around drums which were placed in sterile, airtight plastic bags for storage. This film was used to mould plates of 0.5 mm thickness to use for the moulding of Rogowski test objects (see Section 3.3.2) and plates of 0.25 mm that were placed on teflon shapes in a heating cabinet at 170 °C for 480 hours for oxidation.

3.1.2 Tape

For the purpose of moulding test objects, tape was extruded using a die with 12 mm x 50 mm opening and cut into pieces of ~0.5 m. This tape was later cut into tablets

using a round knife with a diameter of 5.5 cm. The tape was warmed prior to cutting in a heat cabinet at 90 ° C to make it softer and easier to cut.

3.2 Manufacturing Oxidized Particles

Oxidized particles of size 60-110 μm were found in the ROC-2 cable by Sviland [2]. To study the effect of oxidized particles on the breakdown strength of the cable insulation, oxidized particles were manufactured from HDPE-plates of 0.25 mm (see Section 3.3.1).

The plates were placed in a heat cabinet at 170 ° C for 480 hours on teflon shapes to prevent the plates from sticking to the shape upon melting.

The plates were then grinded in a cylindrical metal container containing three metal balls of different sizes. The container was cooled with liquid nitrogen to make the material brittle before being vibrated at 20 Hz for 45 seconds. The grinded material was sieved and sorted into three size categories: 250-355 μm, 100-250 μm and < 100 μm [2].

3.3 Moulding Test Objects

Creating test objects requires working in clean surroundings to avoid intrusion of particles in the objects. Therefore, the objects were prepared for compression moulding on a clean table in filtered air.

3.3.1 Plates

HDPE-plates of 0.5 mm and 0.25 mm were created for the purpose of moulding bottoms onto the rogowski test objects and for creating oxidized HDPE (Section 3.2).

The plates were placed in a mould consisting of three parts: a metal plate, an outer ring, and a shim controlling the thickness of the mould. Film of HDPE (see Section 3.1.1) was cut in 2 cm long strips that were stacked in a star shape in the middle of the mould. A PET-film was placed on top of the moulds (five plates were moulded simultaneously) to ensure that the surface of the HDPE-plate would be smooth.

The plates were moulded using a low pressure cycle and a high pressure cycle as described in Table 3.2. During the low pressure cycle, the material is heated until it melts. In the high pressure cycle, excess material is pushed out to ensure that the plates end up getting the right thickness. The high pressure cycle is followed by ten minutes of cooling.

Table 3.2: Moulding HDPE-plates

Thickness [mm]	T [° C]	Amount of HDPE [g]	Low pressure	High pressure
0.25	130	4.5	2.5 tons/12 min	25 tons/2 min
0.5	9	130	2.5 tons/12 min	25 tons/2 min

3.3.2 Moulding Rogowski Test Objects

Testing insulation material using Rogowski-shaped test objects is easier to control and replicate than to test on full cables. When an electrode has a Rogowski shape, the field strength at the edge of the object is nowhere larger than in the centre, where the field strength is homogeneous [26]. Thus no breakdown will occur at the edges.

A schematic of the mould used to manufacture test objects for this project is shown in Figure 3.2. The mould is comprised of three parts: an outer cylinder (1), a central part (2) which gives the test object its shape and a disk (3) which is pushed against the bottom of the test object. In addition to this, a metal shim was placed on top to set the thickness of the bottom of the object (see Table 3.3).

Tablets of HDPE as those described in Section 3.1.2 were placed between the central part and the disk. To obtain the right amount of HDPE (see Table 3.3), granules of HDPE as those used for extruding (Section 3.1) were placed into the mould before placing the tablet. The granules were carefully pushed down into the mould to avoid creating interfaces near the bottom of the test object. Nine objects were moulded at a time, with an aluminium frame placed around the moulds to prevent heat from escaping during moulding.

A low pressure cycle and a high pressure cycle as described in Table 3.3 were followed by 18 minutes of cooling under high pressure. The quality of the test objects can be quite sensitive to temperature differences. If the temperature overshoots the melting point of the material by a large enough margin, the material will expand sufficiently to stick to the moulds, creating air pockets when the moulds are cooled again.
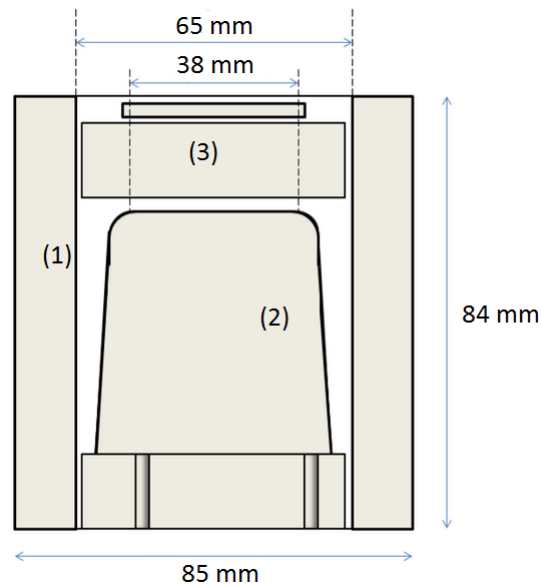
Figure 3.2: Cross-section of the mould used for making Rogowski test objects [2, p. 18]

Table 3.3: Moulding Rogowski Test Objects

Thickness [mm]	Shims [mm]	T [°C]	Amount of HDPE [g]	Low Pressure	High Pressure
0.5	2.8	140	30	2.5 tons /50 min	25 tons /10 min
0.75	2.55	140	-	2.5 tons /50 min	25 tons /10 min

First, objects with 0.5 mm bottom thickness (shims 2.8 mm) were made. For the purpose of moulding bottoms onto the objects, disks of the same radius as the bottom of the test objects were then cut out of the HDPE-plates of 0.5 mm (see Section 3.3.1).

On a third of the test objects, irregularly shaped oxidized particles of size 100-250 μm were placed centrally (on the part of bottom surface with uniform thickness) using a microscope (Figure 3.3b). 10 particles were placed on each object. These objects are referred to as category B test objects in the rest of the report.

Another third of the test objects had irregularly shaped stainless steel particles of 140-250 μm placed centrally (Figure 3.3c). 10 particles were placed on each object. These objects are referred to as category C test objects in the rest of the report.

Finally, on the last third of the test objects, no particles were placed between each moulding (Figure 3.3a). These objects are referred to as category A test objects in the rest of the report.

All the test objects were then put into a mould with a HDPE-plate of 0.5 mm on the bottom. This time shims of 2.55 mm were used, thus getting a total bottom

thickness of 0.75 mm (Table 3.3).

Many objects had to be discarded due to visible air bubbles at the bottom. To remedy this situation, it was tried to use an aluminium foil was wrapped around the object during the second mould. The aluminium foil prevents the HDPE from sticking to the wall during moulding. If the material sticks to the wall during moulding, the result could be air bubbles, typically on the lower part of wall where the insulation is at its thickest. The aluminium foil method was time-consuming, and objects were still discarded due to visible air bubbles on the bottom of the objects when using this method, so it was only used on the category A objects that were DC pre-stressed for 9 (AC tested in the fall semester project [3]) and 163 days.

.

(a) Without particles, category A   **(b)** With oxidized particles, category B   **(c)** With metal particles, category C
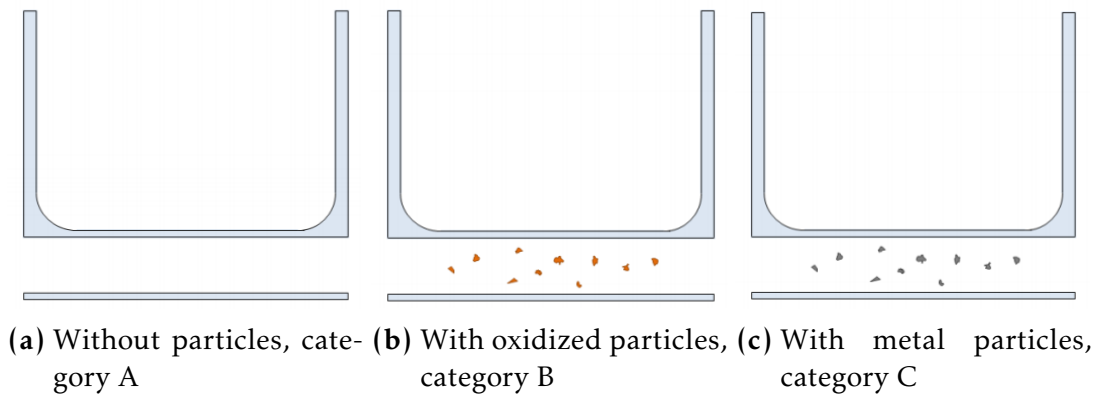
Figure 3.3: Different test object types [2]

A layer of conducting silver paint was painted on the bottom of the object (the part of the object that would be at zero potential) and on the inside of the object (the part of the test object that would be in contact with the electrode) to ensure good electrical contact between the electrode and the insulation material.

Measurements of actual thickness of the test objects: In the fall semester project [3], the thickness of the bottom of all the test objects that were pre-stressed for 0 and 9 days were measured, and the average thickness was found to be 0.75 mm, though with a standard deviance of 0.05 mm (maximum and minimum measured thickness being 0.65 and 0.83 mm). In this work, two objects from each category at each pre-stress level (35 and 163 days) were measured, and similar results were found: average values of 0.75±0.05 mm, with no significant differences between the batches. The small differences in thickness can possibly be attributed to measuring errors.

3.4 DC pre-stress

During type testing, the cable is tested at 100 kV DC for 9 days. To study what effect this DC stress has on the cable, and whether such a field will cause a breakdown in the test objects with contaminations (metal particles and oxidized particles), all the test objects were DC pre-stressed except for 18 AC reference objects, 6 from each category (these were AC-tested to breakdown during the fall semester project [3]) and 15 VLF reference objects, 5 from each category.

The rest of test objects of each type were put under a DC pre-stress in parallel at a voltage level corresponding to the maximum E-field in the cable during type testing. The type test level is 100 kV, and the insulation is 4.7 mm thick. The largest E-field strength occurs at the surface of the inner conductor and can be expressed as [26]:

$$E_{max} = \frac{U}{r ln(\frac{R}{r})} \tag{3.1}$$

where U is the applied voltage, r is the radius of the conductor and R is the radius of the cable. Inserting cable dimensions into Equation 3.1 gives a maximum E-field of 31.49 kV/mm. As the test objects are 0.75 mm thick at the bottom, the DC voltage over the objects was set to 23.6 kV. When applying and turning off the voltage, the level was increased/decreased with a slow rate of roughly 200 V/s to minimize possible effects of fast voltage changes. The voltage was logged every minute using an Agilent logger. The total time spent under DC pre-stress was varied to study the effect of the field over time, see Table 3.4 for a complete test matrix. See Figure 3.4 for a circuit diagram of the DC pre-stress set-up. The 50 kΩ resistance ensured that the rate of voltage change over the test objects would be slowed down in the case of a short-circuit. This because the circuit in Figure 3.4 can be considered as a RC-circuit, where the time constant $\tau = RC$ increases as a function of resistance in the circuit.
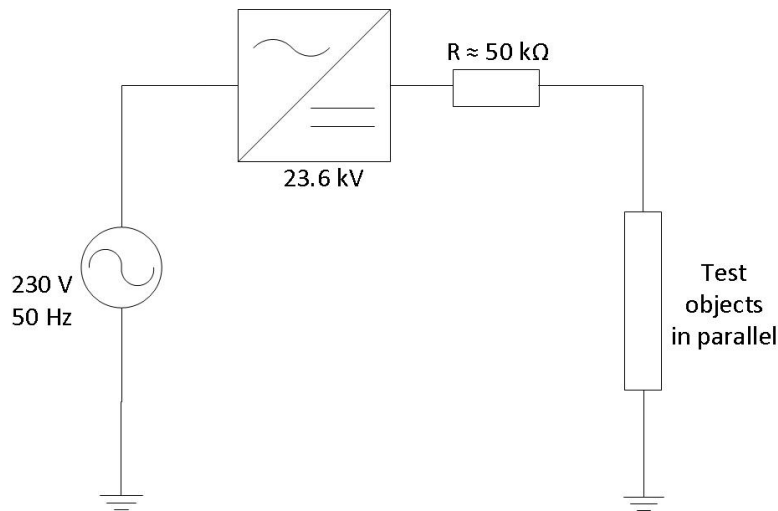
Figure 3.4: Test setup for DC pre-stress.

3.5   Voltage Events

18 objects, 6 from each category, were placed under a long-term DC pre-stress on November 28 2014 at 09:00 and taken out on May 26 2015 at 10:20 (179 days). During this period, due to maintenance and power outages, the voltage was zero during the periods January 27 to February 3 (7 days), February 12 at 22:00 to February 19 at 10:00 (~6,5 days), March 25 at 11:00 to March 26 at 10:00 (1 day), March 30 at 19:00 to March 31 at 08:00 (0,5 days), March 31 at 14:00 to April 1 09:00 (~1 day). This adds up to 16 days, meaning that the total time a DC field was applied to these objects is 179-16=163 days. The voltage loss on March 30 and March 31 also affected the 35-days of prestress objects that were AC-tested. The voltage was set to 26.7 kV by a mistake on February 19 at 10:00, it was reduced to 23.6 kV again on February 24 at 13:15. This event also affected the 35-days of prestress objects that were VLF-tested and the ones that were used for PD measurements.

3.6   AC and VLF Step-up Breakdown Tests

3.6.1   AC and VLF Test Setup

The AC voltage was generated by a 0-220 V 50 Hz adjustable voltage source connected to a 0.22-100 kV transformer (see Figure 3.5). The VLF voltage was generated by 0-66 kV adjustable VLF voltage source, with the frequency set to 0.1 Hz (see Figure 3.6). Test objects with electrodes were placed in silicon oil, and the electrodes were connected to the secondary side of the transformer. Corona rings were placed on the connection points of the transformer and electrodes to avoid corona discharges in the air near sharp edges. The VLF source's maximal output was 66 kV_{rms}.
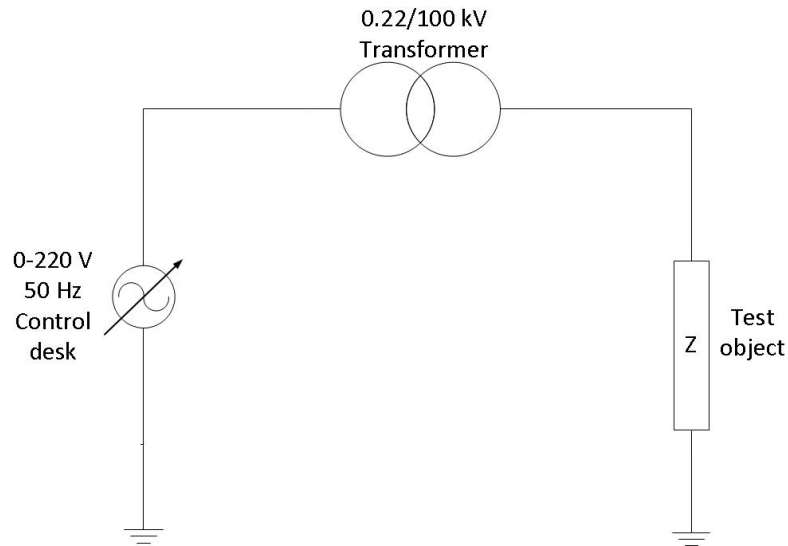
Figure 3.5: Test setup for step-up AC breakdown tests.   Z represents the test object impedance.
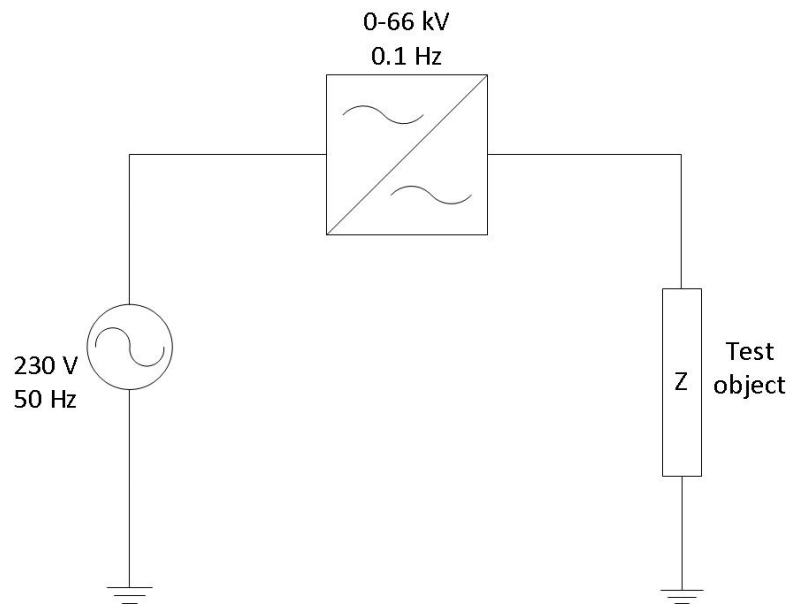

Figure 3.6: Test setup for step-up VLF breakdown tests.   Z represents the test object impedance.

3.6.2   AC and VLF Testing Procedure

To begin with, the voltage was set to 10 kV, and it was subsequently increased by 2.5 kV every 60 seconds. If a breakdown occurred, the voltage was set to zero, and all

conducting parts earthed, and a new test object was placed in the silicon oil.

The breakdown level was noted, and was defined as the last voltage level before breakdown. If there was a breakdown when going from one level to another, the lower voltage level was set as the breakdown level.

3.6.3   AC and VLF Step-up Breakdown Test Program

The purpose of the breakdown tests was to assess whether the 9-day DC pre-stress had an impact on the AC or VLF withstand strength of the insulation material, and whether there would be differences between AC and VLF breakdown strength. The complete test matrix is shown in Table 3.4.

The objects were numbered and randomized by drawing numbers from a hat to randomize the time from the end of the DC prestress to the beginning of the step-up AC/VLF tests. The typical time from earthing the DC voltage over the object to the beginning of the step-up testing was one day.

Table 3.4: Test matrix showing numbers of test objects in each category for AC and VLF step-up breakdown tests and PD measurements.

		Days of DC prestress			
Test type	Object type	0	9	35	163
AC step-up breakdowntests	A	6	6	6	6
	B	6	6	6	6
	C	6	6	6	6
VLF step-up breakdown tests	A	5	-	5	-
	B	5	-	5	-
	C	5	-	5	-
PD measturements	A	2	-	2	-
	B	2	-	2	-
	C	2	-	2	-

3.7   Partial Discharge Measurements

Partial discharges can be measured in several ways, in this work electrical detection with a straight detection circuit was used, see Figure 3.7. The test objects were placed in silicon oil, and a 50 Hz AC voltage was applied. The voltage was increased from 0.5 kV with steps of 0.5 kV (±0.1 kV, the voltage source was not very accurate) every three minutes. When PD inception was observed, the voltage was decreased with 0.5±0.1 kV every three minutes until the extinction voltage was reached. The measurements were made inside a Faraday cage to escape electrical noise from other sources than the test objects.
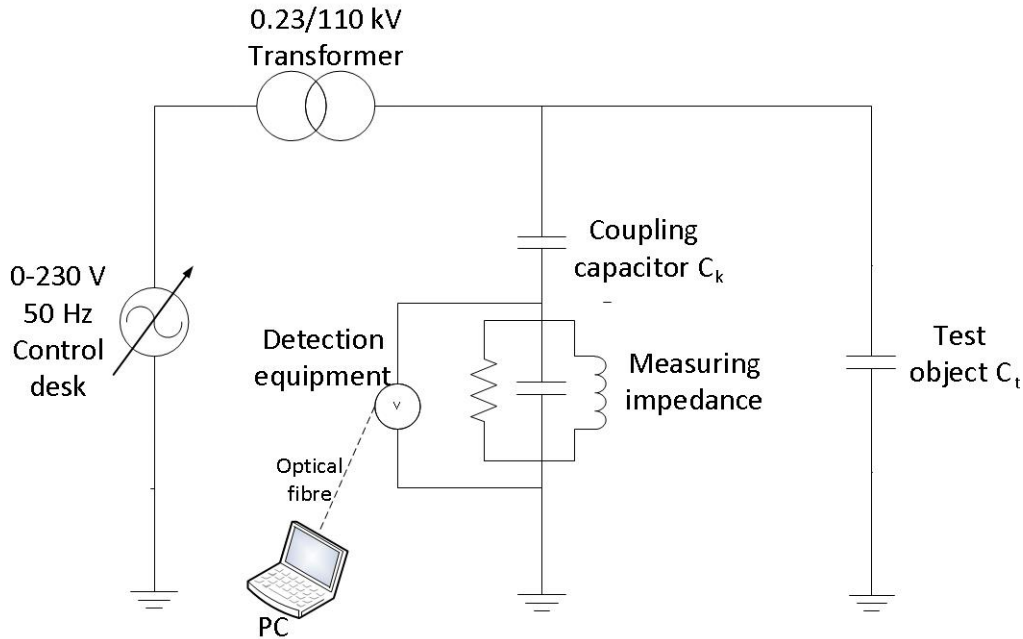
Figure 3.7: Test setup for step-up partial discharge measurements. The capacitance of the coupling capacitor C_k was 800 pF.

PD measurements were performed on two test objects from each category. Measurements were made on the same test objects before and after a 35 days long period of DC pre-stress at 23.6 kV DC. This to see whether the PD inception and extinction voltage would be affected by the DC field. See Table 3.4 for test matrix.

3.8 Pellet Contamination Analysis

3.8.1 Pellet Scanning

23 kg of HDPE pellets were extracted from Nexans Norway's factory in Rognan, which is were the ROC-2 cable is manufactured. The material was extracted as close to the extrusion line as possible, so as to get a realistic sample of the material that goes into the cable.

The pellet were examined with a pellet scanning system (a PS-25C by Optical Control Systems) at Nexans Norways factory in Halden. After the machine had been cleaned with isopropanol, the pellets were fed into a hopper, roughly 1 kg at a time, at a speed of ~130 g/min. The machine then lead the pellets onto a vibrating channel where they were inspected with a high-resolution colour camera for impurities/ colour deviations. By adjusting the aperture of the hopper, the speed with which the pellets were fed into the scanner could be controlled, and thus also the average number of pellets on the vibrating channel.

If no impurities were detected by the camera, the pellets on the vibrating channel would all land in a main box after being scanned. If an impurity in a pellet was detected, the scanner would take a picture of it and divert all the pellets on the vibrating channel into a separate box. The pellets in the main box were fed back into the hopper for a new scan, as the colour camera is only able to detect a contamination when the pellet is orientated in such a way that the camera can see the contamination. Scanning the pellet more than once thus increases the likelihood of discovering all contaminations. After the second scanning, the pellets in the separate box were taken out and examined more closely to single out the pellets with contaminations.

3.8.2   FT-IR Analysis

A Fourier Transform Infrared Spectrometer (FT-IR) was used in order to study the contaminations found in the pellets in Section 3.8.1. The aperture of the microscope was adjusted to 200 by 200 μm (see Figure 3.8a for an illustration of the aperture), and the intensity of the beam was adjusted to ~6250. The microscope was programmed to perform and average 128 separate spectra in the region 4000-580 cm^{-1}.

First, a measurement of the background, i.e. the air, glass in the aperture and other things apart from the sample that the IR beam might hit, was made. Then, microtomed sections of ~25-30 μm of a reference pellet were placed on a KBr disk. KBr is used for IR measurements as it is transparent to IR radiation (IR inactive). Measurements were made of the reference samples to compare with subsequent measurements of microtomed sections of equal thickness (~25-30 μm) of pellets with contaminations. For a schematic of the IR absorption, see Figure 3.8b.
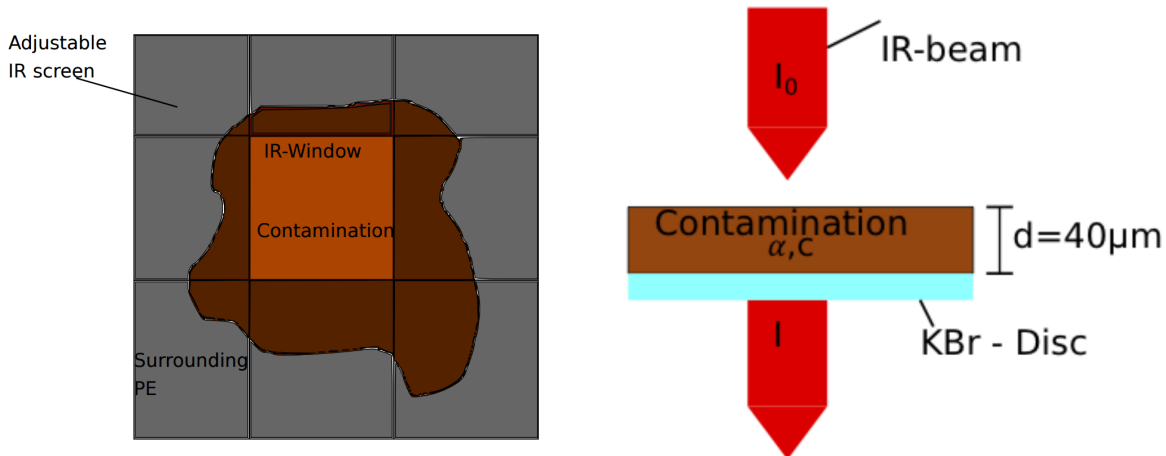
(a) View of a contamination through the FTIR microscope [39]

(b) Schematic of IR absorption in a contamination [39]

Figure 3.8: IR absorption schematic and view of contamination through the spectrometer microscope [39]

The intensity of the spectra can differ slightly due to other factors than the one of interest for analysis of possibly oxidized particles, namely the carbonyl content of the contaminations. Others factors that can attenuate the intensity in the entire frequency range include varying beam intensity and slight differences in sample thickness.

The spectra need to be adjusted (normalized) for this difference, and this is done by identifying a wavenumber at which the reference sample and the sample with a contaminated particle should be equal. The wavenumber chosen was 1897 cm^{-1}, as both contaminated and reference samples appeared to have the same peak in the absorbance spectrum at this wavenumber, so the peak at this wavenumber can be assumed to originate from other factors than carbonyl content.

When two spectra are normalized at 1897 cm^{-1}, this means that the intensity at 1897 cm^{-1} $I_{ref}(1897)$ of a reference should be equal to the intensity of the sample at the same wavenumber $I_{sample}(1897)$. Taking the logarithm of the equality gives $log_{10}(I_{ref}(1897)) = log_{10}(I_{sample}(1897))$, which is equivalent to stating that the absorbance spectra $A_{ref} = log_{10}(\frac{I_0}{I_{ref}})$ and $A_{sample} = log_{10}(\frac{I_0}{I_{sample}})$ should be equal at 1897 cm^{-1}, assuming that the intensity I_0 that the reference and sample are subjected to is equal. Therefore, the absorbance spectra were used to normalize the spectrum of each sample to that of a reference sample. This was done in Matlab by multiplying the entire absorbance spectrum of the sample by the ratio between A_{ref} and A_{sample} at 1897 cm^{-1} (code in Appendix F).

4 Results

4.1 DC pre-stress

No breakdown of any test object occurred during the DC pre-stress.

4.2 AC Step-up Breakdown Tests

Table 4.1 shows the results of the AC breakdown tests, with the results for 0 and 9 days of pre-stress from [3]. All objects had a breakdown through the object's bottom as expected, except for one test object in category A without DC pre-stress, which had a breakdown through the side of the object at 56.67 kV/mm. Even though breakdown mostly happened through the object bottom, the breakdown often occurred near the side wall. This could be a result of the polymer sticking to the wall during moulding, leading to air bubbles. Note the especially high breakdown strength of category A and B objects after 163 days of prestress. The complete data set of AC breakdown strengths of the test objects is appended in appended in Table D.1 in Appendix D.

Table 4.1: AC breakdown strength results. All values in kV_{rms}/mm.

Days of DC pre-stress	Category	E_{min}	E_{max}	E_{avg}	standard deviation σ
	A	23.3	56.7	40.6	13.7
0	B	23.3	53.3	35.0	13.1
	C	20.0	40.0	28.9	6.6
	A	26.7	46.7	37.8	7.2
9	B	30.0	36.7	32.2	3.4
	C	26.7	36.7	31.1	4.0
	A	26.7	40.0	32.2	5.4
35	B	26.7	46.7	37.8	8.1
	C	16.7	36.7	28.9	7.5
	A	46.7	73.3	63.3	10.1
163	B	33.3	76.7	63.3	17.0
	C	33.3	40.0	36.7	3.7

4.2.1 Weibull Probability Plots

To assess whether the breakdown data could come from a Weibull distribution, the parameters $E_{63.2}$ and β of the Weibull distribution were estimated. The value $E_{63.2}$ is the E-field at which $1 - \frac{1}{e} \approx 63.2$ % of the samples are estimated to have failed, and β is the slope of the cumulative probability function, which is a straight line in a Weibull probability plot. A low β means that there is a lot of scatter in the results and vice versa.

The x-axis in the Weibull plot represents the breakdown E-field and the y-axis shows the estimated cumulative probability of failure $P(E)$ at the given E-field. The formula for the Weibull cumulative probability distribution is [26]:

$$P(E) = 1 - e^{-(\frac{E}{E_{63.2}})^{\beta}} \tag{4.1}$$

Rearraging and taking the natural logarithm on both sides of Equation 4.1 twice gives a straight line with slope β:

$$ln(-ln(1 - P(E))) = \beta lnE - \beta lnE_{63.2} \tag{4.2}$$

The parameters β and $E_{63.2}$ and thus the line in Equation 4.2 are estimated with linear regression in SigmaPlot. The cumulative probabilities for each sample are found with the approximation [4]

$$P(E_i) \cong \frac{i - 0.3}{n + 0.4} \times 100\% \tag{4.3}$$

where i is the sample number, ordered from lowest to highest breakdown strength, and n is the sample size.

The Weibull probability plots of the different samples in Table 4.1 are presented in Figures 4.1 to 4.2. As the number of samples in each category is small (6 in each), 95 % confidence limits for the estimated Weibull distribution are included in all figures. These are constructed from the 95 % confidence limits of the parameters $E_{63.2}$ and β. Confidence limits express the fact that the real distribution with great probability lies within the area bounded by the limits (the confidence interval). If the tests were repeated a large number of times, and each time a confidence interval was calculated, then 95 % of the confidence intervals would contain the true distribution.

When comparing tests, one can conclude that one category of samples is significantly better at the given confidence level than another if their confidence intervals are not overlapping [26].

Figures 4.3, 4.4 and 4.5 compare the effect of 0, 35 and 163 days DC pre-stress within each category (data for 0 days of prestress from earlier work by the author [3]), while Figures 4.1 and 4.2 compare the effect of contaminants with 35 and 163 days of DC pre-stress respectively.
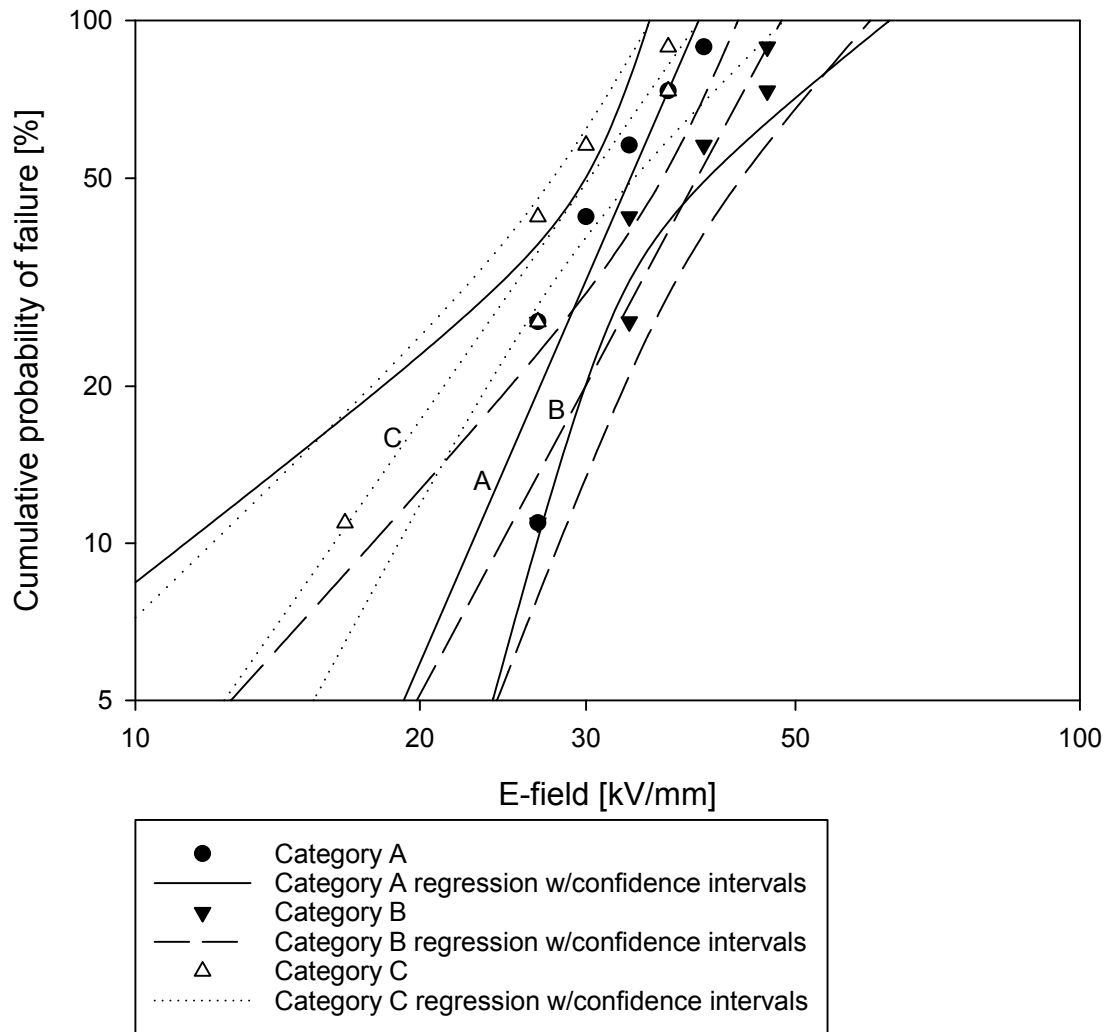
Figure 4.1: Weibull probability plot of AC withstand strength of test objects after 35 days of DC pre-stress with 95 % confidence intervals.
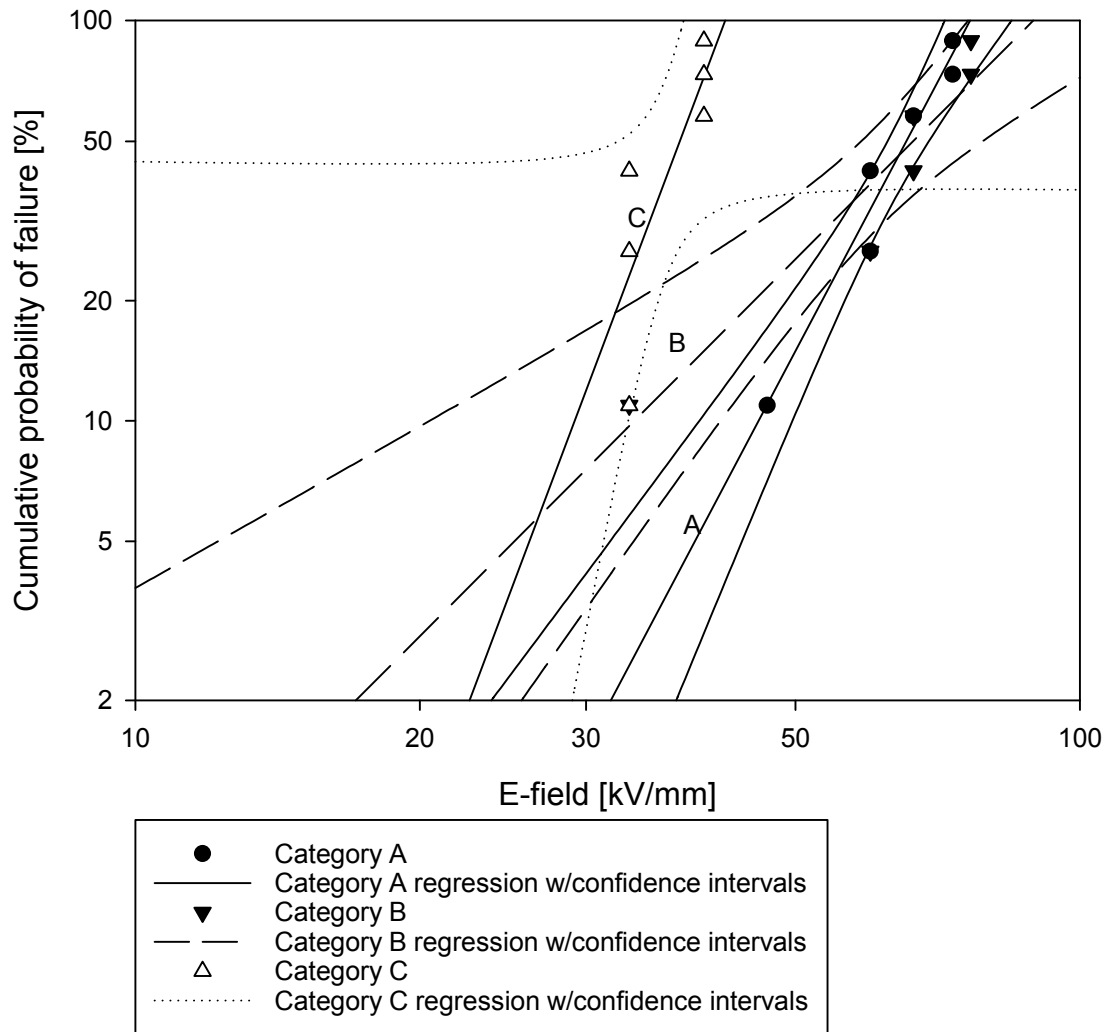
Figure 4.2: Weibull probability plot of AC withstand strength of test objects after 163 days of DC pre-stress with 95 % confidence intervals.
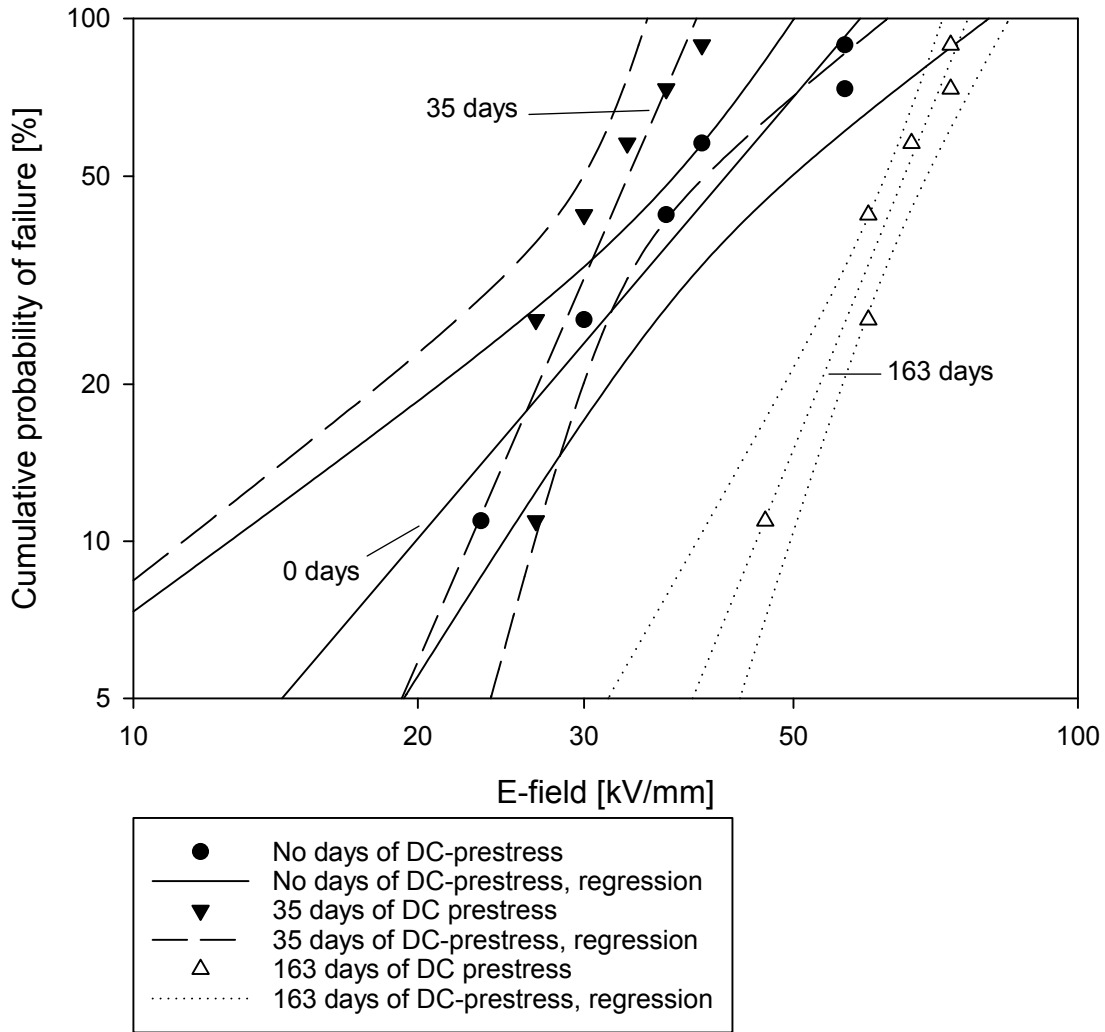
Figure 4.3: Weibull probability plot of AC withstand strength of category A objects after 0 (data from [3]), 35 and 163 days of DC pre-stress with 95 % confidence intervals.
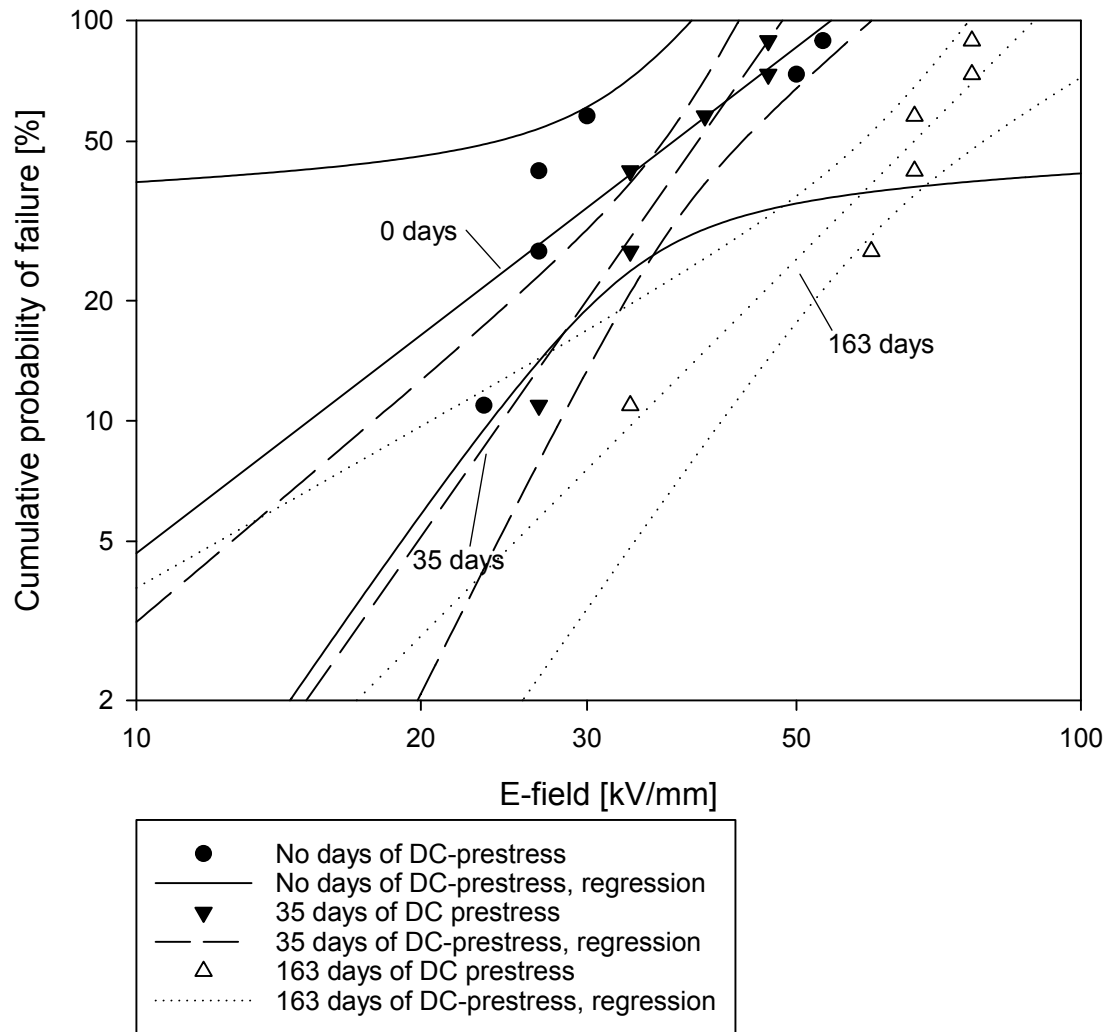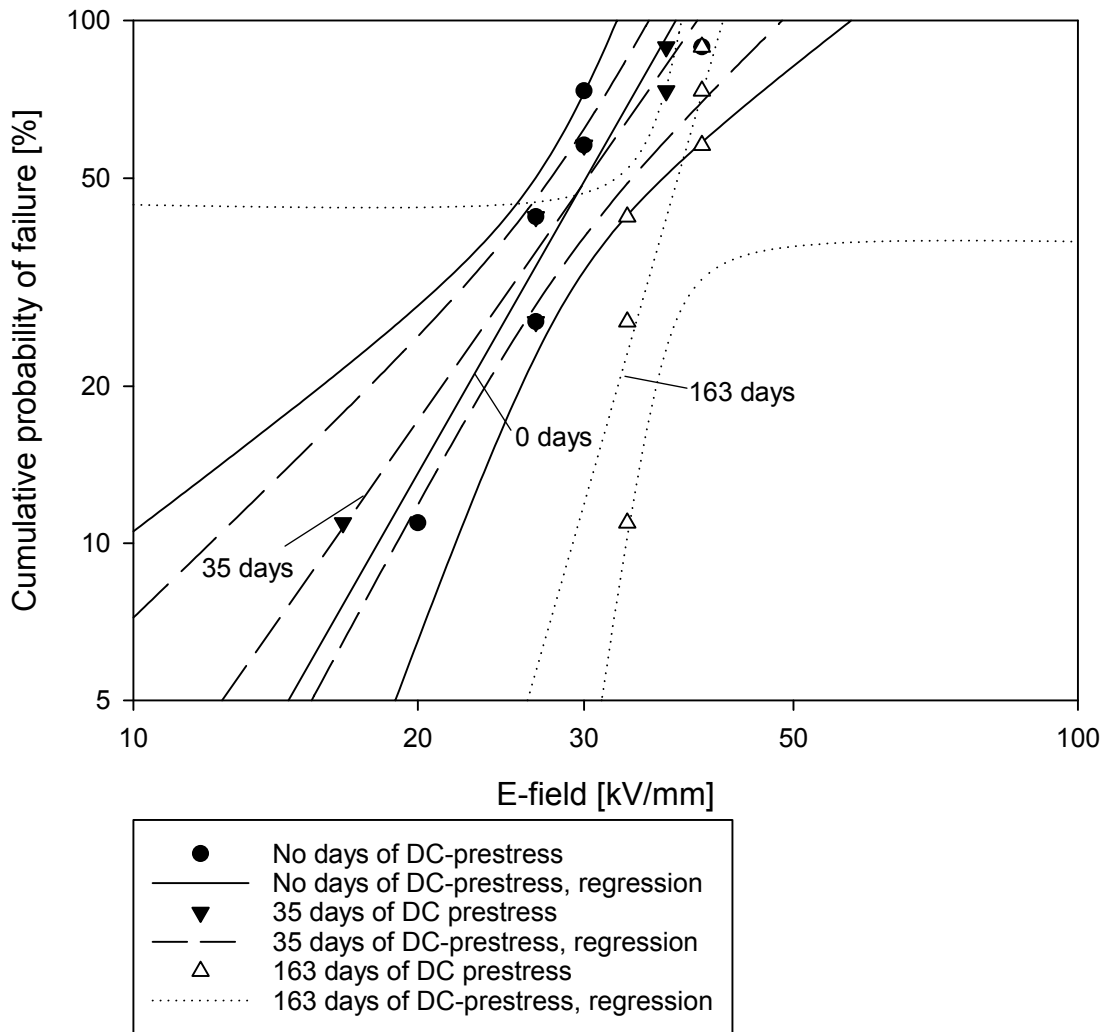
Figure 4.4: Weibull probability plot of AC withstand strength of category B objects after 0 (data from [3]), 35 and 163 days of DC pre-stress with 95 % confidence intervals.

Figure 4.5: Weibull probability plot of AC withstand strength of category C objects after 0 (data from [3]), 35 and 163 days of DC pre-stress with 95 % confidence intervals.

4.2.2   Life Plots: Effect of DC pre-stress on AC step-up breakdown strength

The life plots in Figures 4.6, 4.7 and 4.8 were made using SigmaPlot and show the estimated $E_{63.2}$ values of the AC breakdown strength with 95 % confidence intervals (calculated using the Matlab function wblfit()) of category A, B and C objects after 0, 9, 35 and 163 days of DC pre-stress. Note that the regression line in Figure 4.6 is well outside the 95 % confidence limit of the objects that were DC pre-stressed for 35 days.
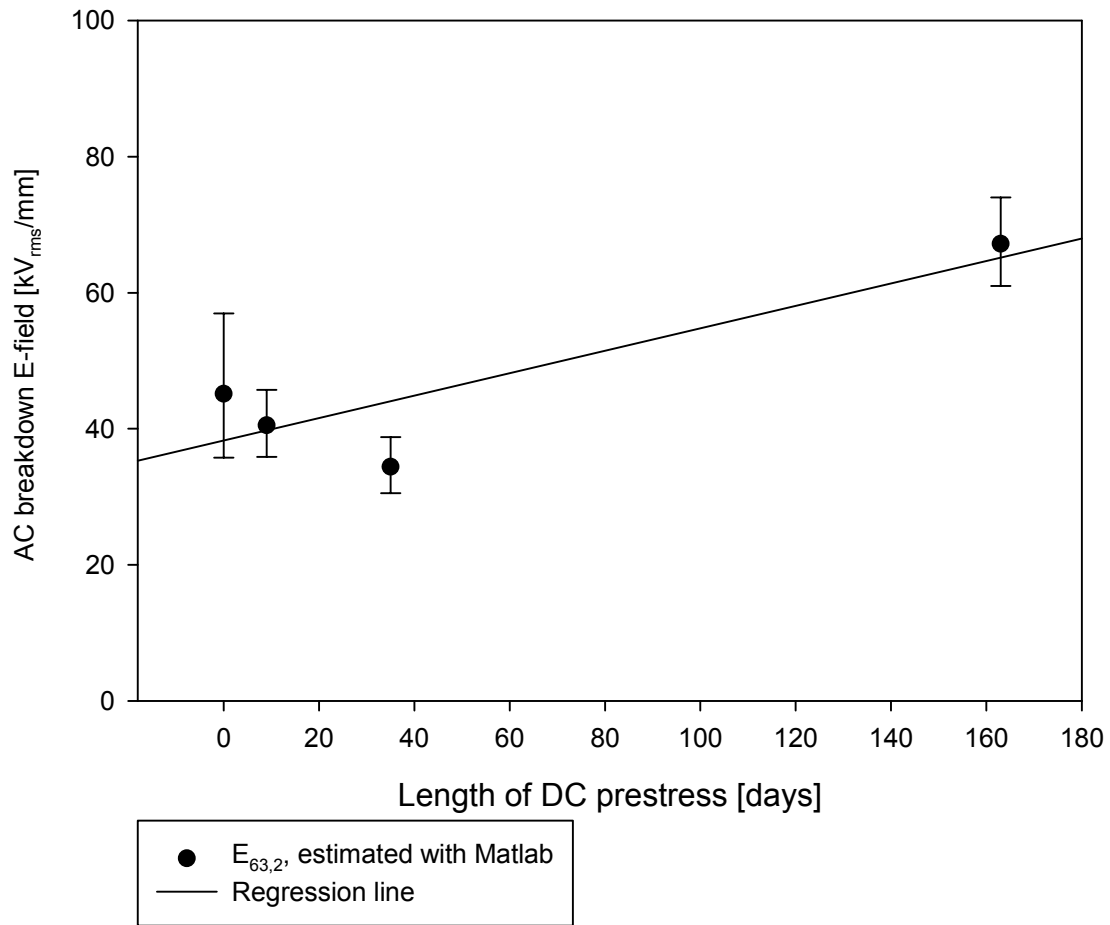
Figure 4.6: $E_{63.2}$ AC breakdown values with 95 % confidence intervals of category A objects after various lengths of DC pre-stress.
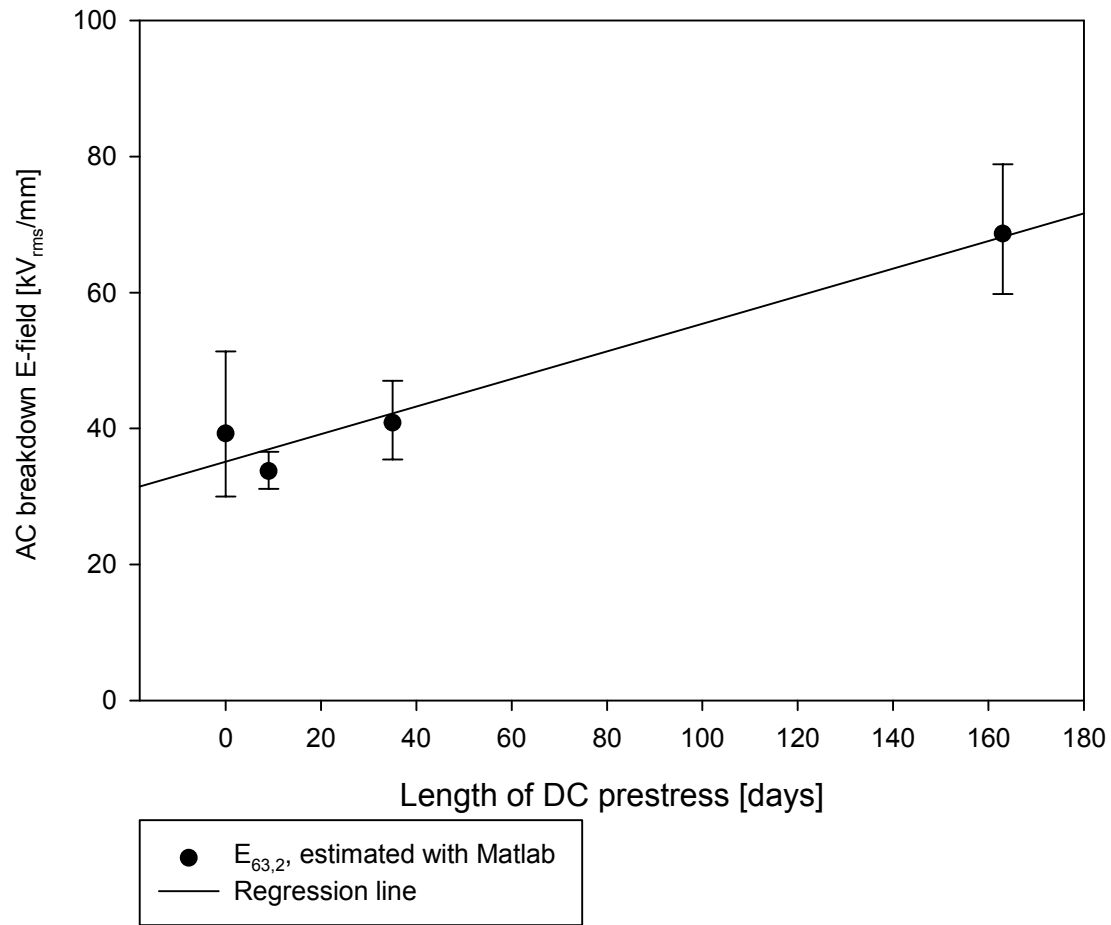
Figure 4.7: $E_{63.2}$ AC breakdown values with 95 % confidence intervals of category B objects after various lengths of DC pre-stress.
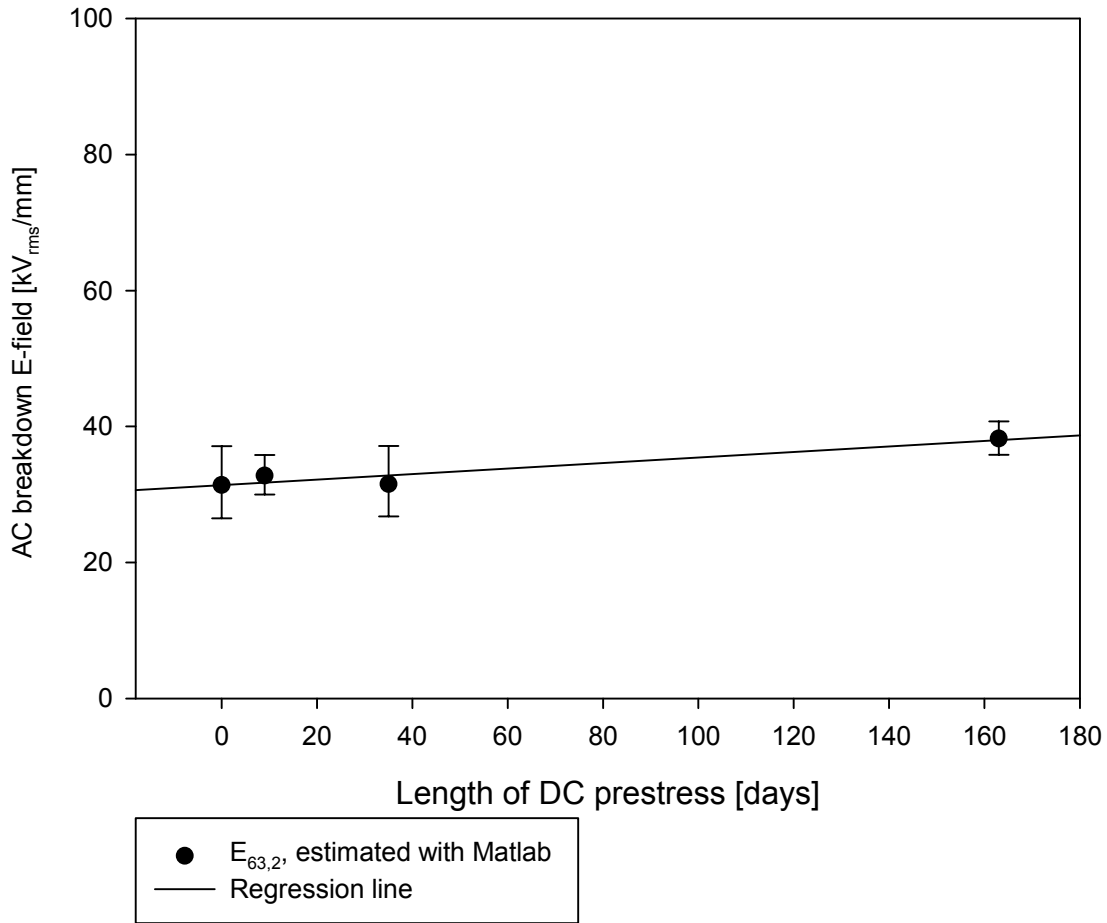
Figure 4.8: $E_{63.2}$ AC breakdown values with 95 % confidence intervals of category C objects after various lengths of DC pre-stress.

4.3 VLF Step-up Breakdown Tests

The results of the VLF step-up breakdown tests are presented in Table 4.2. As none of the objects that were not pre-stressed experienced breakdown (right-censored data only), it was not possible to use Weibull statistics to analyse the results.

Table 4.2: 0.1 Hz VLF step-up breakdown voltages in kV_{rms}/mm

| Object category | Breakdown field strength [kV$_{rms}$/mm] | |
	Without DC prestress	With DC prestress (35 days)
	>88	66.7
	>88	>88
A (no particles)	>88	>88
	>88	>88
	>88	>88
	>88	>88
	>88	>88
B (oxidized particles)	>88	>88
	>88	>88
	>88	>88
	>88	83.3
	>88	83.3
C (metal particles)	>88	>88
	>88	>88
	>88	>88

4.4 Partial Discharges

The inception and extinction voltages of two objects of each category before and after a DC pre-stress of 35 days (DC pre-stress level 31.5 kV/mm) is shown in Table 4.3. Figure E.1-E.3 in Appendix E show PD activity at inception voltages of a test object from each category before and after the pre-stress period. The discharge pattern is typical to that of cavities in dielectrics, but it could also come from surface discharges as these are not distinguishable (see Figure 2.9).

Table 4.3: PD inception and extinction AC field strengths before and after 35 days of DC pre-stress in kV_{rms}/mm (rounded to the nearest 0.5 kV step).

| Object | Days of DC pre-stress | | | | Change [%] | |
| | 0 days | | 35 days | | | |
	Inception	Extinction	Inception	Extinction	Inception	Extinction
A1	6.7	4.7	2.0	1.3	-70%	-72%
A2	6.7	5.3	2.7	2.0	-60%	-62%
B1	6.7	4.7	6.7	4.7	0%	0%
B2	6.7	5.3	2.0	1.3	-70%	-75%
C1	7.3	3.3	2.7	2.0	-64%	-40%
C2	8.0	4.0	2.0	1.3	-75%	-67%

4.5   Pellet Contamination Analysis

4.5.1   Pellet Scanning, Microscopic Analysis and Contamination Classification

15 internal contaminations were found. They were all of brown and black colour and near the surface, some even partly on the surface.

A measure of the longest side of the pellet revealed an average value of 256,7 μm and a standard deviation of 85,4 μm. Figure 4.9 show some pellets with contaminations, see Appendix B.1 for pictures of all pellets with contaminations.
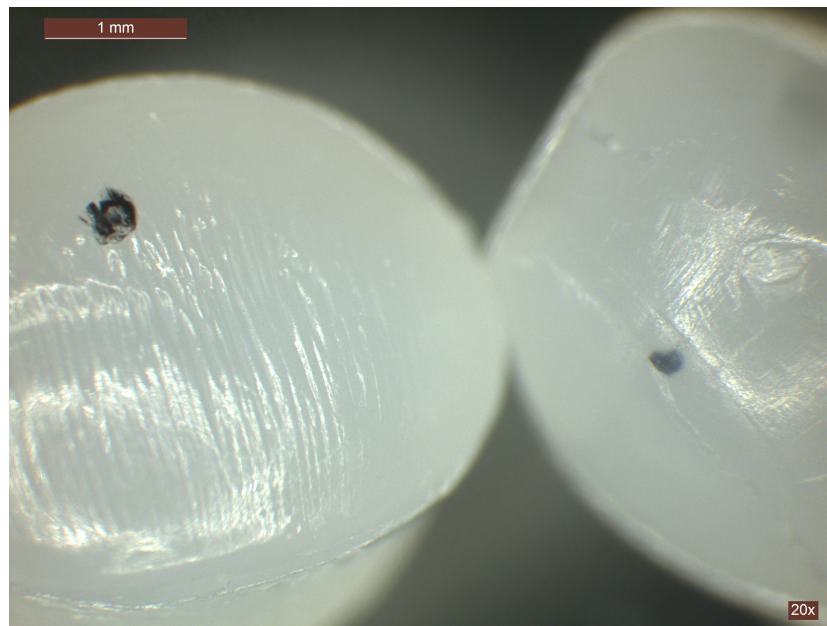

Figure 4.9: Two pellets with contaminations.

The pellets were microtomed, and the microtome sections were studied further under a microscope. With the later spectral analysis in mind, the contaminations were classified into three different categories based on their colour (see Figure 4.10). Pictures of microtomed sections of all contaminations found are appended (Appendix B.2).

(a) Category 1   **(b)** Category 2
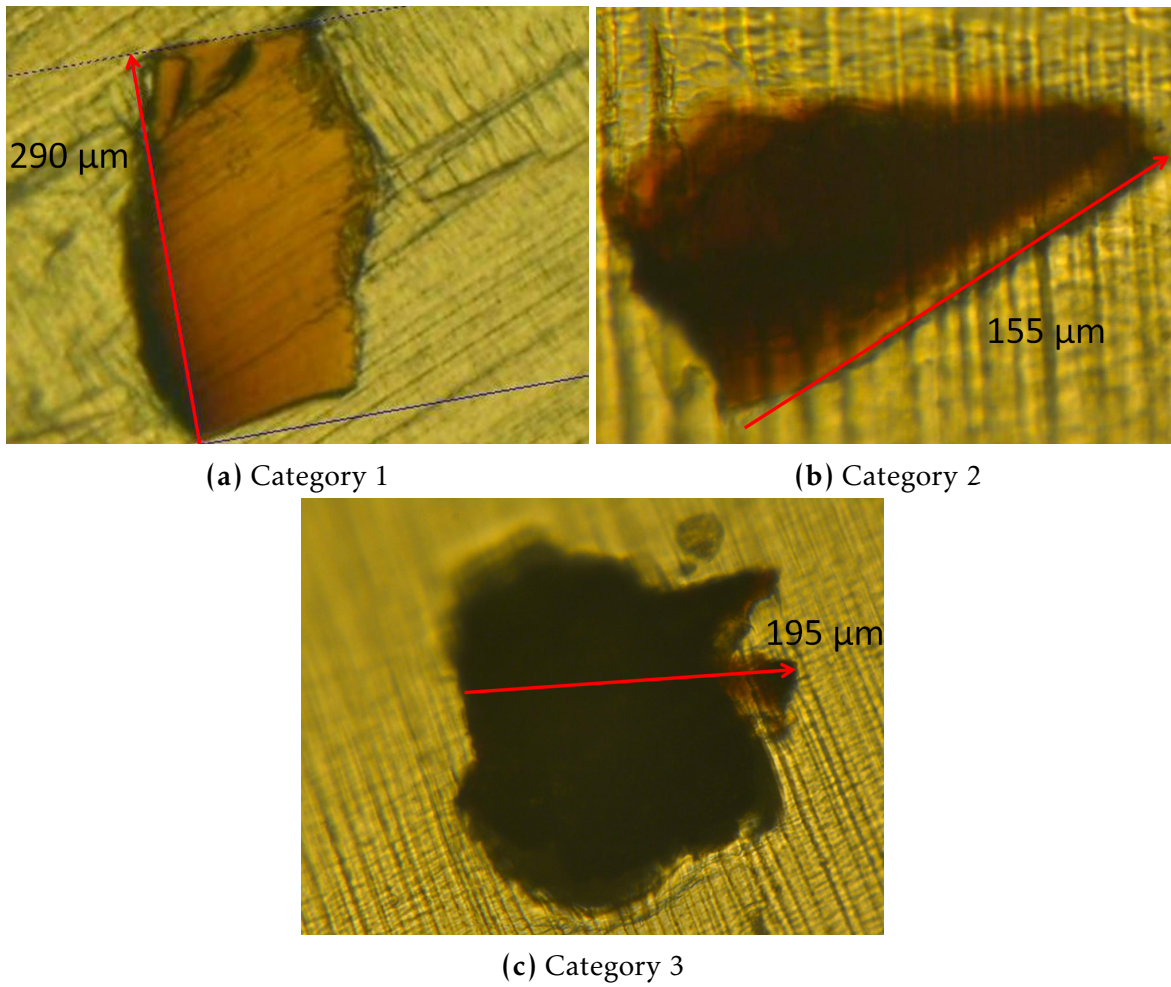
(c) Category 3

Figure 4.10: Microtomed contaminations illustrating categories of contaminations found in HDPE pellets

4.6 FT-IR Analysis

Below are examples of IR spectra from each category in Figure 4.10. 12 spectra of contaminations (3 classified as category 1, 4 as category 2 and 5 as category 3) were obtained, and they are all appended in Appendix A. In all figures of spectra, the 1897 cm^{-1} normalized contamination sample (solid line) is compared with the same sample of reference PE (dotted line) of roughly the same thickness.

4.6.1 Category 1

Figure 4.11 shows the IR spectrum of a category 1 contamination. Some salient absorption peaks have been highlighted. Of special interest to the degree of oxidation are the carbonyl compounds at 1745-1710 cm^{-1}, these are also present in the other two category 1 contaminations spectra. In the carbonyl group absorption peak, two smaller peaks at ~1739 cm^{-1} and ~1711 cm^{-1} can be distinguished. There appears to be absorption in the sample in the region between ~1300-900 cm^{-1} in all category 1 spectra, especially in the spectra in Figure 4.11. This region is known to be complex, with bands originating in interacting vibrational modes, such as CH$_2$ twisting and wagging (see Table 2.2). There is probably influence from the C-O streching vibrations of alcohol (OH) groups, known to produce a strong band in the 1260-1000 cm^{-1} region. Ketones also show moderate absorption in the 1300-1100 cm^{-1}

$$\overset{\displaystyle O}{\underset{\displaystyle \|}{}}$$

region as a result of C-C-C stretching and bending in the C——C——C group, and C-O stretching vibrations of esters also result in an absorption band in this region [36]. There is also more absorption in the region 3400-3200 cm^{-1} in the contamination sample in Figure 4.11 than the reference, which is a typical absorption band for bonded OH groups [36].
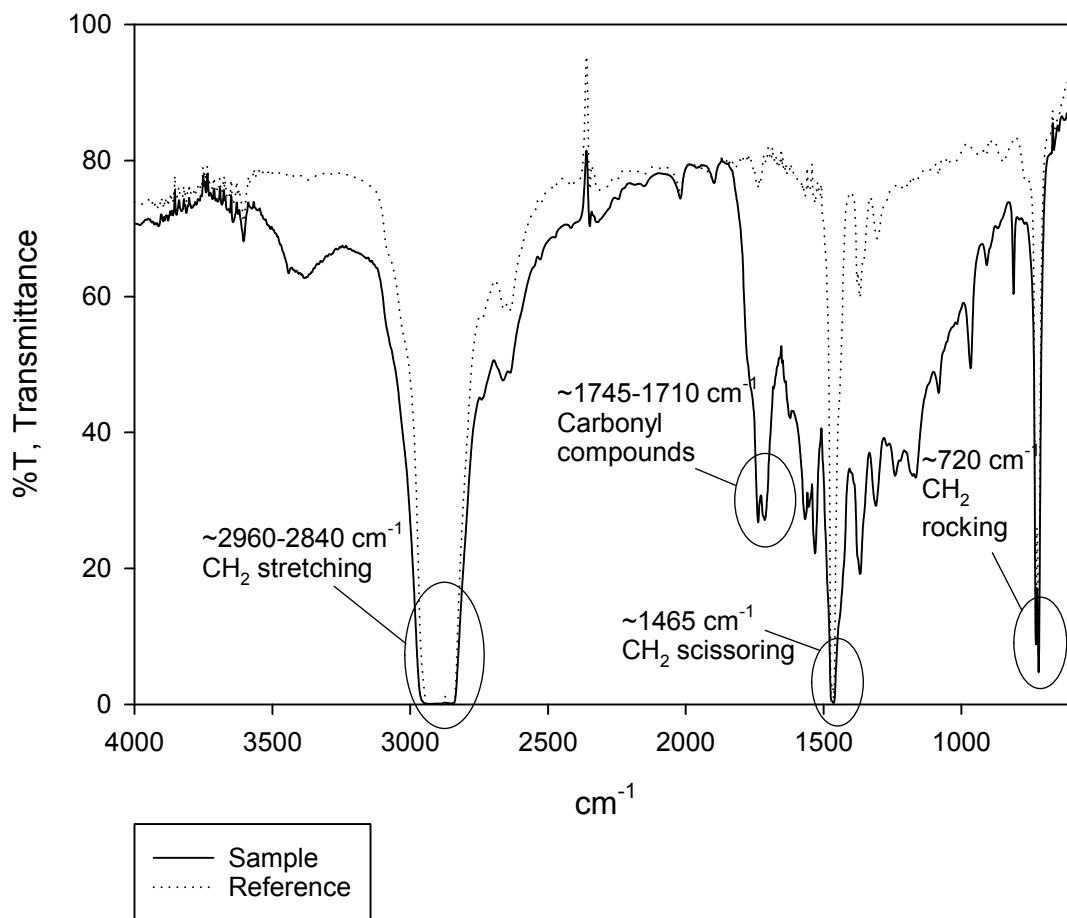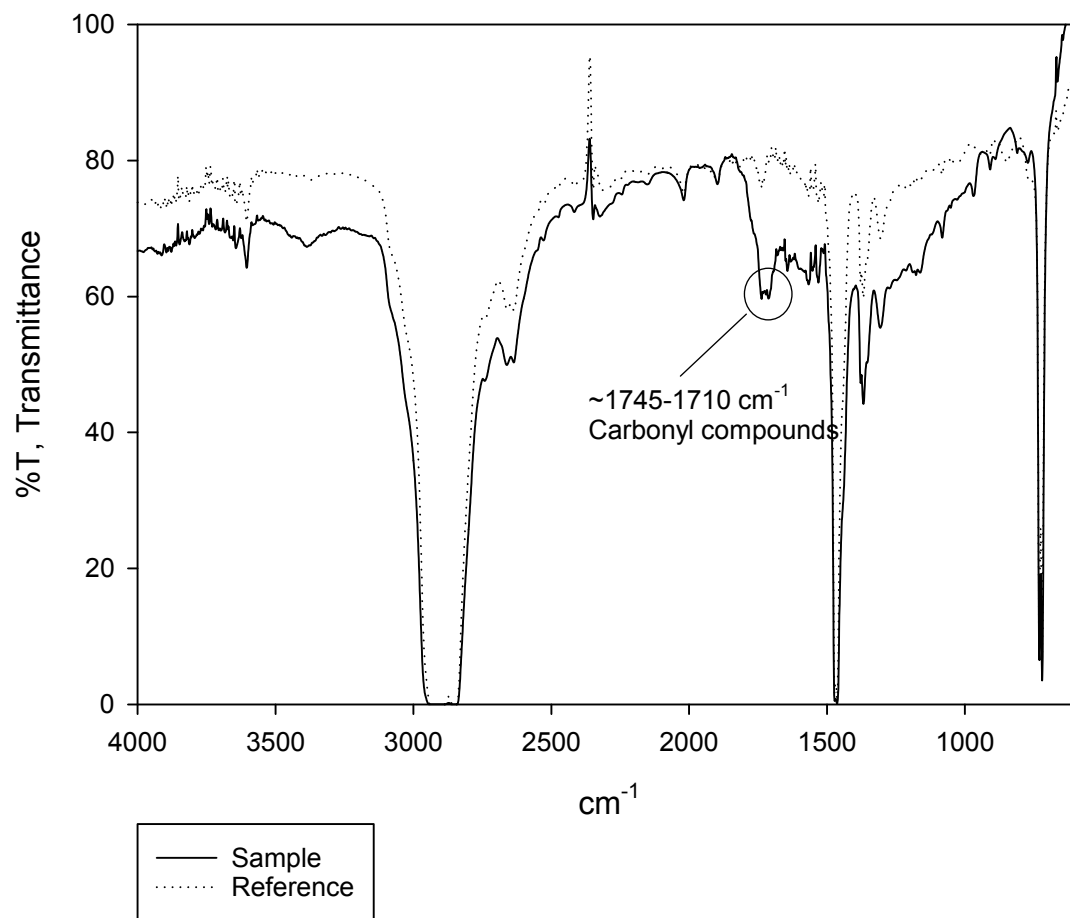
Figure 4.11: FT-IR transmittance spectrum of the category 1 contamination in Figure 4.10a.

4.6.2 Category 2

Figure 4.12 shows the IR spectrum of a category 2 contamination. The absorption peaks due to CH_2 stretching, scissoring and rocking can also be seen in Figure 4.12, but are not highlighted as in Figure 4.11. There is an absorption peak indicating carbonyl compounds (highlighted). Again the carbonyl absorption peak seems to have two smaller peaks at ~1739 cm^{-1} and ~1711 cm^{-1}. One other category 2 spectra (Figure A.5) also have carbonyl absorption peaks, while two (Figures A.6 and A.7) do not stand out from the reference sample.

Figure 4.12: FT-IR transmittance spectrum of the category 2 contamination in Figure 4.10b.

4.6.3   Category 3

Figure 4.13 shows the IR spectrum of a category 3 contamination. A possible carbonyl absorption peak at 1711 cm^{-1} (possibly ketone or carboxylic acid) has been highlighted. One other spectrum of category 3 contaminations exhibit carbonyl absorption peaks (Figure A.11), while the remaining three are not discernible from the reference spectrum (Figures A.9, A.10 and A.12).
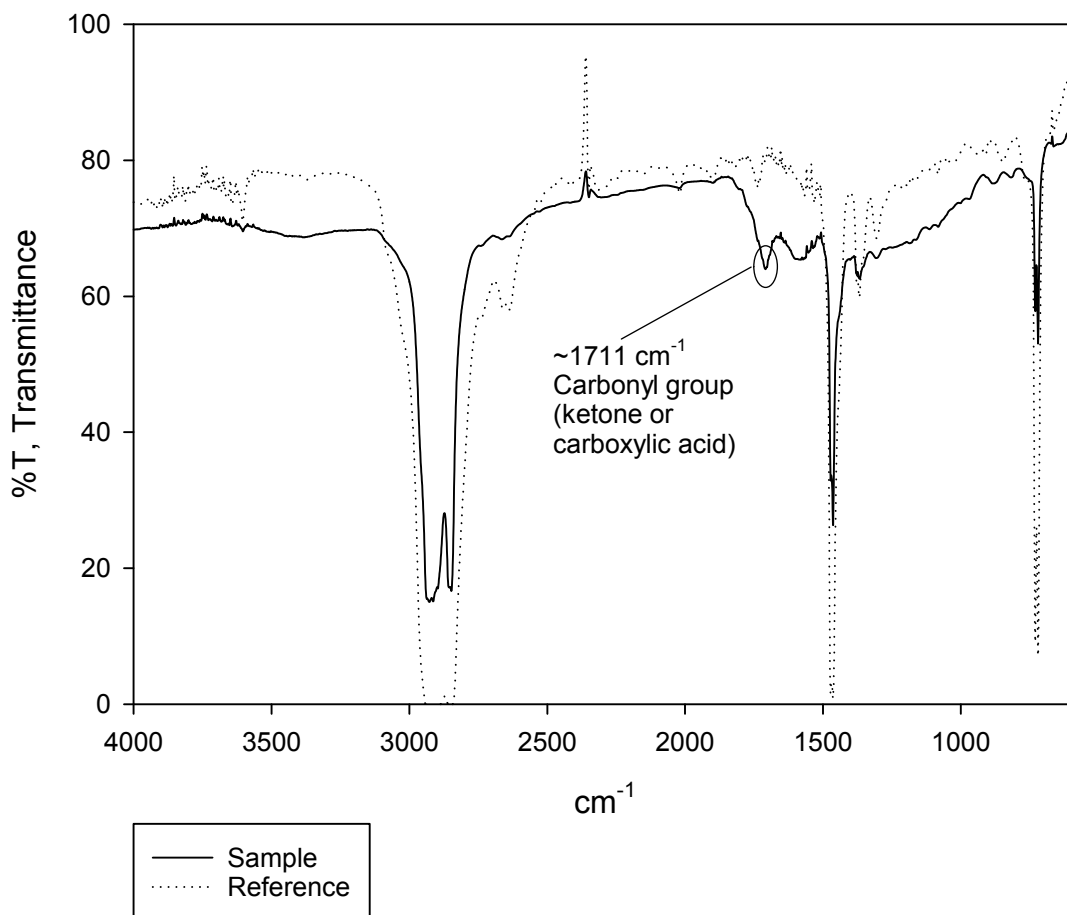
Figure 4.13: FT-IR transmittance spectrum of the category 3 contamination in Figure 4.10.

4.6.4   Carbonyl Group: Absorbance Spectra

Figure 4.14 shows the absorbance spectra around the carbonyl region of the three contaminations in Figure 4.10c. There is a general broadening of the carbonyl region in all spectra except for the reference. Category 1 has the most salient peaks, these

have been investigated further, and the likely origin has been highlighted. Saturated aliphatic ketones (i.e. non-aromatic ketones), which are the likely ketones to be expected in the samples in Figure 4.14 as polyethylene is non-aromatic, have a "normal" absorption frequency at 1715 cm^{-1} [36]. Such a peak can be seen in Figure 4.14. Aliphatic aldehydes absorb near 1740-1720 cm^{-1}, and such a peak is also observed in Figure 4.14. There are peaks in these areas for category 2 and category 3 as well, although the category 3 sample seems to lack a strong aldehyde peak. The peaks in the 1570-1530 cm^{-1} region of the category 1 contamination have been assigned to carboxylate anions (RCOO-), these are known to absorb near 1650-1550 cm^{-1} and 1400 cm^{-1} [36]. There is a distinguished peak at ~1535 cm^{-1} which is just outside the 1650-1550 cm^{-1} carboxylate anion region. There is a possibility that this peak could be due to antioxidants, this will be discussed more in Section 5.6.2. The category 1 contamination in Figure 4.14 has spectral similarities to category 3 contaminations in [39]. There is absorption in the 1570-1530 cm^{-1} region for the category 2 and category 3 sample as well, indicating carboxylate anions in these contaminations as well.

Even though Figure 4.14 seems to indicate a significant difference between the categories, similar differences were found within each category in the carbonyl group. See Figures A.13-A.15 for comparisons of carbonyl region absorbance within each category.
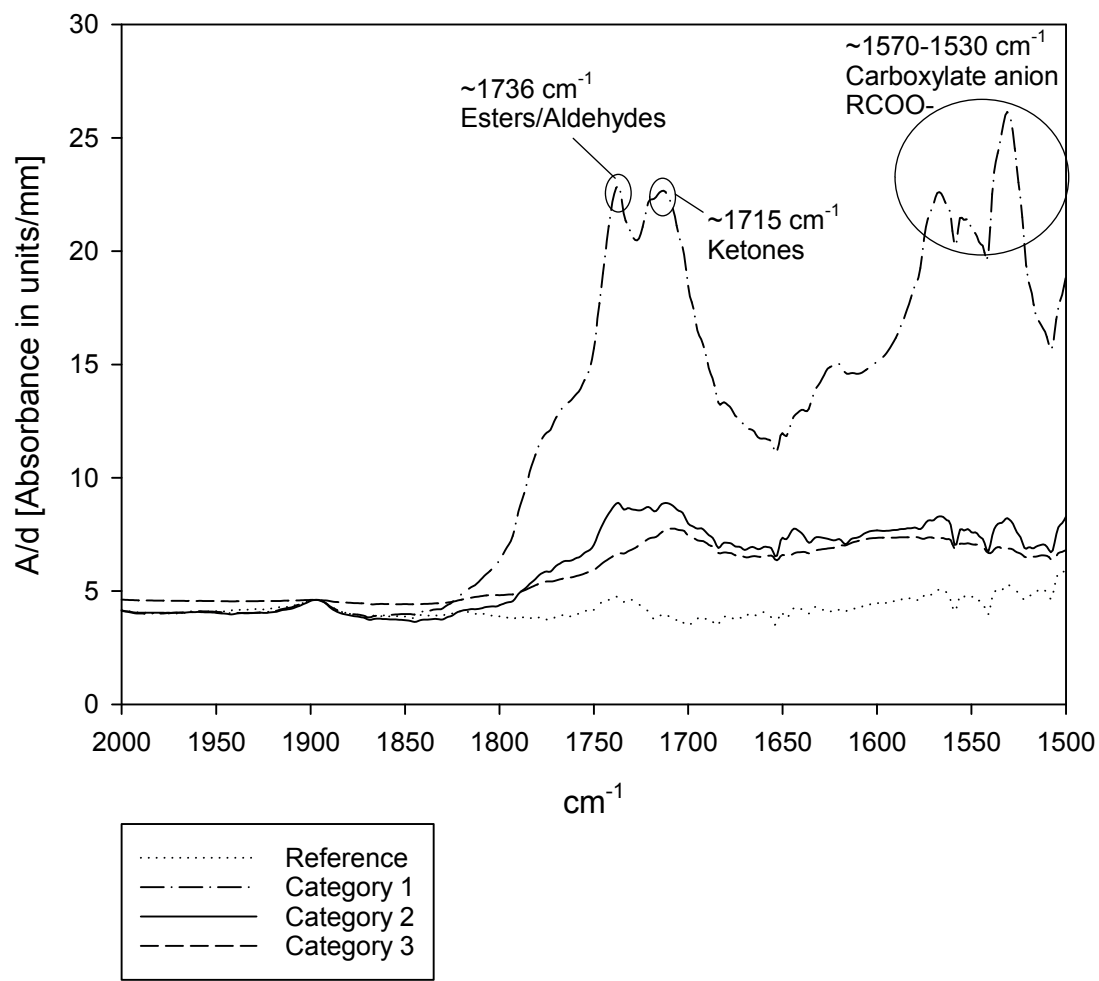
Figure 4.14: FT-IR absorbance spectra of the carbonyl region of the three contaminations in Figure 4.10c.

5 Discussion

5.1 AC Withstand Strength After DC Pre-stress

Figures 4.3, 4.4 and 4.5 show no significant change in the insulation's AC withstand strength after DC pre-stress, as the confidence intervals are overlapping. The exception is a significant increase in AC breakdown strength between category A objects with 35 and 163 days of pre-stress, the latter having the significantly higher breakdown strength.

The category B objects that were pre-stressed for 163 days also have a very high breakdown strength (63.3 vs. 37.8, 32.2 and 35.0 kV_{rms}/mm for category B objects with 35, 9 and 0 days of pre-stress respectively, see Table 4.1), but a larger spread (standard deviation of 16.95 kV_{rms}/mm) ensure that the 95 % confidence intervals are overlapping.

These results lead to life plots that indicate an increase in the AC breakdown strength with time of DC pre-stress of category A and B objects, see Figures 4.6 and 4.7. The same can not be concluded for category C objects, but the DC pre-stress doesn't seem to have a negative effect on the AC withstand strength of these objects either.

It seems unlikely that a longer DC pre-stress would strengthen the insulation material's ability to withstand AC fields. A reason for the high breakdown strength of the 163 days category A objects could be that these objects were produced using an aluminium foil. However, these objects experienced breakdown at a greater average value (63.3 vs. 37.8 kV_{rms}/mm, see Table 4.1) than the category A objects that were DC pre-stressed for 9 days and produced the same way, so the effect of the aluminium foil on the AC breakdown strength is questionable. The thickness of the conducting paint can also play a role in the withstand strength of the objects. All the objects that were subjected to 163 days of pre-stress received a new layer of paint before AC testing. This was not done for other objects, except for the ones that were used for PD measurements.

There is generally a large spread within categories too, with an average standard deviation of 8.3 kV_{rms}/mm at each cell in the test matrix (see Table 3.4 and Table 4.1). This could be explained by small differences in the manufacturing. Objects placed at the edge during moulding experience lower temperatures than objects placed in the centre, even with an aluminium screen placed around the objects. HDPE in objects that are moulded at higher temperatures will stick more to the moulds than objects moulded at lower temperatures, and are more likely to create voids when the material is cooled again. Another factor is the lack of semiconductors on the objects. A layer of semiconductor between the insulation and the electrodes would have evened out the field more, probably leading to less variation in breakdown strength.
.

5.2   VLF Withstand Strength After DC Pre-stress

The results in Table 4.2 indicate that the withstand strength of the objects is at least 2 to 3 times higher than the AC withstand strength at the same level of pre-stress. 90 % of the data is right-censored, with only three test objects experiencing breakdown, making it impossible to analyse the data with Weibull statistics. The higher breakdown strength at 0.1 Hz VLF was expected, as 0.1 Hz VLF has been shown to require 2 to 3 times higher voltage to eliminate similar defects in a comparable time [30].

5.3   Partial Discharges

The results in Table 4.3 indicate that the PD inception and extinction field strength decreases with length of DC pre-stress. The inception field strength is reduced by an average of 56.5 % after a 35-day pre-stress. One test object (B1) shows no change in inception or extinction voltage. The discharge patterns in Figures E.1-E.3 could also come from surface discharges, as the conducting paint was not evenly distributed. Parts of the paint came off every time the electrode was put in contact with the test object in the silicon oil. The test objects were coated with a new layer of paint and the experiments were repeated several times, but parts of the paint always came off, making it impossible to know whether the discharges were internal discharges or surface discharges.

The lowest inception fields in Table 4.3 are 2.0 kV/mm. Assuming a flat cavity (highest field amplification, see Section 2.3.3), the field will be ϵ_r times higher: $\epsilon_r \cdot 2 = 2.3 \cdot 2 = 4.6$ kV/mm. It can then be seen from the modified Paschen curve in Figure 2.7 that the cavity must be roughly 0.25 mm, assuming atmospheric pressure as will be the case after some time of air diffusion. Sviland [2] found cavities of up to 200 μm in a sample of the ROC-2 cable, but it seems unlikely that cavities of such a size would not be visible on the bottom of the Rogowski test objects. Considering this and the conducting paint's bad adhesion to the insulation, it seems very likely that the discharges measured were surface discharges and not internal discharges.

5.4   Effect of Contaminants on AC and VLF Breakdown Strength After DC Pre-stress

No significant difference in the AC breakdown strength between objects with particles and objects without has been found (see Figures 4.1 and 4.2 and [3]). The average AC breakdown value of category A objects (43.5 kV/mm) is only slightly higher than the average AC breakdown value of category B objects (42.1 kV/mm) and both are higher (38.5 % and 34 % respectively) than the average breakdown value of category C objects (31.4 kV/mm) (see Table 4.1).

According to [7], typical AC breakdown strength of HDPE insulating material is 100 kV/mm, but the average value for objects without contaminants at all pre-stress

levels found in this work was 43.5 kV/mm. Sviland's [2] tests found an average breakdown strength of 67.1 kV/mm for similar objects (the objects used in [2] were 1 mm, not 0.75 mm as in this project). The relatively low AC breakdown value could be a result of interfaces and entrapment of air near the bottom of the cup formed when the PE granules melted together or other manufacturing errors. The effect of the interface created when the objects were moulded a second time could be another explanation [2].

The VLF data was too right-censored to analyze with Weibull statistics (see Table 4.2). Of the three breakdowns that occurred, 1 was a category A object (at 66.7 kV/mm), the other 2 were category C objects (both at 83.3 kV/mm).

The cable insulation is placed on the seabed and is in direct contact with the sea. The effect of moisture in the insulation has not been studied in this report, but it does seem to reduce the breakdown strength of the insulation [2].

5.5   Quality of the Type Test

If it is assumed that the inverse power law relation in Equation 2.22 with n in the range of 6.9 to 11.6 as have been found for joint mouldings [32] is relevant for the cable, the estimated life of a cable that can withstand 100 kV DC for 9 days is much longer than the expected service life of 25 years.

However, the relation in Equation 2.22 might be relevant for AC voltages, but not necessarily for DC as it does not take into account the time-dependence of the effective stress under DC. The equivalence between ramped tests and constant stress tests at DC is thus questionable. Relevant operating stresses such as rapid groundings and the presence of contaminants are likely to be the limiting factors of the cable lifetime, and a fundamental understanding of the features specific to DC fields is important if the statistical data are to be interpreted with confidence [4].

In the fall semester project [3], the test objects were analyzed to determine the size and orientation of the particles that were inserted into the insulation. The biggest metal particle found in the insulation bridged ~40 % (312.69 μm) of the insulation thickness in the field direction, which is a severe flaw that could lead to breakdown in the cable lifetime.

As the same electric field as in the 9-day type test (31.5 kV/mm, ten times the operating field) doesn't seem to accelerate the tested breakdown processes of such severe defects in the insulation after 163 days, the ability of the test to eliminate the types of irregularities that have been found in the raw material and those that have been found by Sviland [2] in manufactured cable lengths is questionable.

5.6 Pellet Contamination Analysis

5.6.1 Pellet Scanning and Microscopic Analysis

The pellet scanning revealed 15 internal contaminants of various shades of brown and black in 23 kg of raw material. The method doesn't guarantee that any pellet contaminant would be found, even if all the material was screened twice. Some contaminants will be too deep in the pellet to be seen by the camera, and some pellets with contaminants could have been oriented the wrong way both times for the camera to see the contaminant.

5.6.2 FT-IR Analysis

Category 1: The three spectra of category 1 contaminants (see Figure 4.11 and Appendix A.1) all have clear absorption peaks around wavenumbers 1745-1710 cm^{-1}, which are typically associated with the stretching vibrations of the carbonyl group C=O, which is an indicator of PE oxidation (see Section 2.6.2). The two smaller peaks that are discernible in the carbonyl group peak in the spectra at 1736 and 1715 cm^{-1} indicates that there are likely different types of molecules with the carbonyl group, such as esters, ketones, aldehydes and carboxylic acids (see Table 2.3).

Alcoholic groups also accumulate during thermooxidative degradation [37]. The C-O stretching vibration in the alcohol can explain the increased absorption of the contaminated sample in the region 1300-900 cm^{-1} in Figure 4.11. The increased absorption in the 3400-3200 cm^{-1} region also indicates the presence of alcohol, as bonded OH groups are known to have a strong absorption band in this region. There is similar evidence of alcohol groups in the other two category 1 spectra (Figures A.2 and A.3), but this is not as clear as in Figure 4.11.

Category 2: Two category 2 spectra (Figure 4.12 and A.5) have carbonyl absorption peaks which indicate oxidation, while two (Figures A.6 and A.7) do not stand out from the reference sample. The fact that the latter don't show signs of oxidation is surprising, as all the contaminations look like oxidized material (see Figure B.2) and are roughly the same size. The aperture of the IR beam was however 200 by 200 μm, which is slightly larger than the particles, and this, combined with slight variations in sample thickness and thickness and density of the contaminations could be a source of error.

Category 3: Two category 3 spectra have carbonyl absorption peaks which indicate oxidation (Figure 4.13 and A.11), while the remaining three are not discernible from the reference spectrum (Figures A.9, A.10 and A.12). The same sources of error as for category 2 spectra apply.

Possible antioxidants in the 1570-1530 cm^{-1} region: In Figure 4.14, the peak at 1535 cm^{-1} is outside the carboxylate anion (RCOO-) band, which is known to absorb near 1650-1550 cm^{-1} [36].

Typical antioxidants in polyethylene are aromatic [40] and skeletal vibrations in the ring of aromatics are known to absorb in the 1600-1300 cm^{-1} region [36], which could explain the 1535 cm^{-1} peak. The probability of antioxidants being responsible for the peak is however low since the amount of additives in polymers is very small (0.1-1 % [40]), although additivites in polymer cables have been found to aggregate into clusters of ∼25 μm under certain conditions without electric stresses [4].

6   Conclusions

The aim of this work has been to investigate the effect of a long-term DC field on the insulation material used in repeatered optical cables (ROC) cables. The following conclusions are made:

- FT-IR characterization of 15 internal contaminants of black and brown colour found in the cable insulation raw material has produced spectra similar to those one would expect for oxidized PE.

- A DC field corresponding to ten times the operating field of the ROC-2 cable for 0, 9, 35 and 163 days on HDPE Rogowski test objects with different contaminations (oxidized and metal particles of size $\sim 100 - 480$ μm [3]) does not deteriorate the AC breakdown strength of the insulation significantly.

- The same DC field for 35 days does not seem to reduce the VLF withstand strength of the insulation material significantly. The test objects' average VLF breakdown strength is at least 2-3 times as high as the AC average breakdown strength.

- These results indicate that the 9-day 100 kV DC test that is used as a type test for the ROC-2 cable doesn't accelerate any of the tested breakdown processes that could lead to failure of the cable, and the ability of the test to detect the types of irregularities that have been found in the raw material and those that have previously been found in manufactured cable lengths [2] is therefore questionable.

- Small sample sizes and a large spread within each category of test objects has made it difficult to obtain significant results, although it was observed that objects without contaminants that had been stressed with a DC-field for 163 days had a significantly higher breakdown strength than similar objects stressed at 35 days. This is likely due to manufacturing variations as it is hard to conceive a physical explanation for an increase in breakdown strength with time of DC pre-stress.

- The partial discharge (PD) inception voltage of test objects of all categories decreases with an average of 56.5 % after a 35 day DC pre-stress, although there are likely measuring errors in that the discharges measured could be surface discharges and not internal discharges since the conducting paint consistently came off during PD testing.

7 Recommendations for Further Work

VLF: VLF could be used in the routine tests for the ROC-2 cable to detect defects of the insulation. Establishing a correlation between AC and VLF for the cable insulation could be useful in the development of test methods. This was tried in this thesis, but the VLF source was not able to achieve high enough voltage levels to induce breakdown in the samples that weren't pre-stressed and in most of the samples that were. The effect of a long-term DC field on the VLF breakdown strength will also be of interest.

Scanning electron microscope (SEM) investigation of defects: A scanning electron microscope (SEM) produces images of a sample by scanning it with a focused beam of electrons. SEM pictures of the contaminants found in the cable raw material would indicate the presence of voids at the interface between the contaminant and the particle. This information would be valuable to understand the field phenomena occurring near the contaminants.

Joints: In general electric breakdown is a weakest link mechanism [30], and in cables such as the ROC-2, regions of amalgamations in joints could be such a weak link because of the discontinuities introduced in the insulation system with injection moulding techniques [32]. Therefore, it could be interesting to do electrical and acoustical partial discharge (PD) measurements of joints, and cut out and visually inspect the areas of the joints where there are PDs.

Cable with physical damage: Testing on cable sections where parts of the insulation have been removed or damaged could be interesting to simulate the effect of exterior damage to the insulation. The insulation of the ROC-2 cable is very thick, and failure of the cable is most likely to occur in cases where the insulation has been severely damaged. Applying a high DC voltage over time to such a cable could indicate whether such a damage would be critical for the cable's lifetime.

References

[1] K. Thyagarajan and A. Ghatak, *Fiber optic essentials*. John Wiley & Sons, 2007, vol. 10.

[2] E. Sviland, "Utvikling av testmetoder for fiberoptisk sjøkabel med dc-drevne forsterkere," Master's thesis, NTNU, 2014.

[3] H. K. H. Meyer, *Project work: development of test mesthods for a combined dc power and fiber optic deep water cable*. NTNU, Department of Electric Power Engineering, 2014.

[4] L. A. Dissado and J. C. Fothergill, *Electrical degradation and breakdown in polymers*. IET, 1992, no. 9.

[5] A. Barlow, "The chemistry of polyethylene insulation," *Electrical Insulation Magazine, IEEE*, vol. 7, no. 1, pp. 8–19, 1991.

[6] F. H. Kreuger, *Industrial high DC voltage: 1. fields, 2. breakdowns, 3. tests*. Delft University Press, 1995.

[7] E. Ildstad, *High Voltage Insulation Materials*. NTNU, Department of Electric Power Engineering, 2012.

[8] J. Bostrom, A. Campus, R. Hampton, and U. Nilsson, "Evaluation of the material reliability for polymeric direct current cables," *CIGRE Report*, pp. 15–404, 2002.

[9] G. Mazzanti and M. Marzinotto, *Extruded Cables for High-Voltage Direct-Current Transmission: Advances in Research and Development*. John Wiley & Sons, 2013, vol. 93.

[10] S. Hvidsten, M. Vandbakk, and F. Mauseth, "Dielectric properties of organic contaminations in xlpe cable insulation," in *Electrical Insulation and Dielectric Phenomena (CEIDP), 2012 Annual Report Conference on*. IEEE, 2012, pp. 684–687.

[11] T. Mizutani and M. Ieda, "Carrier transport in high-density polyethylene," *Journal of Physics D: Applied Physics*, vol. 12, no. 2, p. 291, 1979.

[12] P. Fischer and P. Röhl, "Transient currents in oxidized low-density polyethylene," in *Mehrphasige Polymersysteme*. Springer, 1977, pp. 149–153.

[13] G. Kavafian, "Observations on the behavior of linear polyethylenes derived from heat degradation studies," *Journal of Polymer Science*, vol. 24, no. 107, pp. 499–501, 1957.

[14] B. Baum, "The mechanism of polyethylene oxidation," *Journal of Applied Polymer Science*, vol. 2, no. 6, pp. 281–288, 1959.

[15] W. Hawkins, "Thermal and oxidative degradation of polymers," *Polymer Engineering & Science*, vol. 4, no. 3, pp. 187–192, 1964.

[16] T. Kelen, *Polymer degradation*. Van Nostrand Reinhold Co., 1983.

[17] W. Thue, R. Lyle *et al.*, "The origin and effect of small discontinuities in polyethylene insulated urd cables," *Power Apparatus and Systems*, *IEEE Transactions on*, no. 7, pp. 2116–2123, 1983.

[18] M. S. Khalil, "International research and development trends and problems of hvdc cables with polymeric insulation," *Electrical Insulation Magazine*, *IEEE*, vol. 13, no. 6, pp. 35–47, 1997.

[19] S. Boggs, "Very high field phenomena in dielectrics," *Dielectrics and Electrical Insulation*, *IEEE Transactions on*, vol. 12, no. 5, pp. 929–938, 2005.

[20] M. Selsjord and E. Ildstad, "Electrical treeing caused by rapid dc-voltage grounding of xlpe cable insulation," in *Electrical Insulation*, *2006. Conference Record of the 2006 IEEE International Symposium on*. IEEE, 2006, pp. 502–505.

[21] R. Densley, R. Bartnikas, and B. Bernstein, "Multiple stress aging of solid-dielectric extruded dry-cured insulation systems for power transmission cables," *Power Delivery*, *IEEE Transactions on*, vol. 9, no. 1, pp. 559–571, 1994.

[22] H. R. Gnerlich, "Field testing of hv power cables: understanding vlf testing," *Electrical Insulation Magazine*, *IEEE*, vol. 11, no. 5, pp. 13–16, 1995.

[23] M. Ytterstad, "Kvalitetssikring av polymerisolerte hvdc kabler ved hjelp av spenningsprøving," Master's thesis, NTNU, 2008.

[24] E. Ildstad, F. Mauseth, M. Selsjord, R. Hegerberg, and Z. Xiao, "Quality control of extruded hvdc cables: Detection of critical flaws using low frequency voltage endurance testing," *Gaodianya Jishu/ High Voltage Engineering*, vol. 37, no. 11, pp. 2664–2671, 2011.

[25] F. Mauseth, E. Ildstad, R. Hegerberg, M. Jeroense, B. Sanden, and J. E. Larsen, "Evaluation of abrupt grounding as quality control method for hvdc extruded cables," in *Electrical Insulation and Dielectric Phenomena*, *2008. CEIDP 2008. Annual Report Conference on*. IEEE, 2008, pp. 41–44.

[26] F. Kreuger, "Industrial high voltage: electric fields, dielectrics, constructions," *Delft University Press, Delft, The Netherlands*, 1991.

[27] P. H. Morshuis, "Degradation of solid dielectrics due to internal partial discharge: some thoughts on progress made and where to go now," *Dielectrics and Electrical Insulation, IEEE Transactions on*, vol. 12, no. 5, pp. 905–913, 2005.

[28] F. Kreuger, "Industrial high voltage: co-ordinating, measuring, testing," *Delft University Press, Delft, The Netherlands*, 1991.

[29] H. Suzuki, K. Aihara, and T. Okamoto, "Complex behaviour of a simple partial-discharge model," *EPL (Europhysics Letters)*, vol. 66, no. 1, p. 28, 2004.

[30] F. Mauseth, E. Ildstad, M. Selsjord, and R. Hegerberg, "Quality control of extruded hvdc cables: Low frequency endurance testing of model cables with contaminations," in *High Voltage Engineering and Application (ICHVE), 2010 International Conference on*. IEEE, 2010, pp. 136–139.

[31] G. Chen and A. Davies, "The influence of defects on the short-term breakdown characteristics and long-term dc performance of ldpe insulation," *Dielectrics and Electrical Insulation, IEEE Transactions on*, vol. 7, no. 3, pp. 401–407, 2000.

[32] L. Dissado, I. Doble, S. Wolfe, P. Norman, A. Davies, G. Chen, Q. Zhong, W. Wargotz, and M. Sanders, "Electrical reliability of dc-operated submarine telecommunications cables," *Dielectrics and Electrical Insulation, IEEE Transactions on*, vol. 4, no. 1, pp. 1–9, 1997.

[33] M. Brown, G. Chen, A. Daies, L. Dissado, and P. Norman, "Space charge characterization in aged ldpe amalgamated insulation regions from underwater telecommunication systems," *Dielectrics and Electrical Insulation, IEEE Transactions on*, vol. 7, no. 3, pp. 346–352, 2000.

[34] D. Whittaker, *Interpreting organic spectra*. Royal Society of Chemistry, 2000.

[35] N. Colthup, *Introduction to infrared and Raman spectroscopy*. Elsevier, 2012.

[36] R. Silverstein and F. Webster, *Spectrometric identification of organic compounds*. John Wiley & Sons, 2006.

[37] A. Holmström and E. M. Sörvik, "Thermooxidative degradation of polyethylene. i and ii. structural changes occurring in low-density polyethylene, high-density polyethylene, and tetratetracontane heated in air," *Journal of Polymer Science: Polymer Chemistry Edition*, vol. 16, no. 10, pp. 2555–2586, 1978.

[38] G. Socrates, *Infrared and Raman characteristic group frequencies: tables and charts*. John Wiley & Sons, 2004.

[39] M. Vandbakk, "Organic contaminations in sub-marine ac and dc high-voltage cables," Master's thesis, NTNU, 202ss.

[40] R. B. Walter and J. F. Johnson, "Analysis of antioxidants in polymers by liquid chromatography," *Journal of Polymer Science: Macromolecular Reviews*, vol. 15, no. 1, pp. 29–53, 1980.
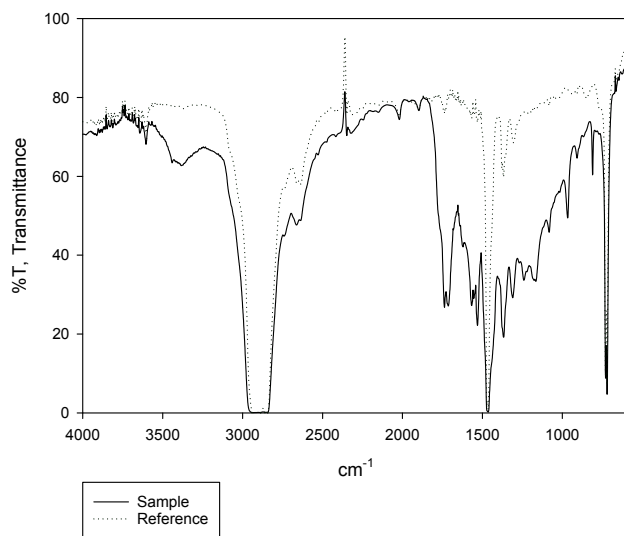
A FT-IR Spectra

A.1 Category 1

Figure A.1: FT-IR spectrum of a category 1 contamination (second picture, second row in Figure B.2).
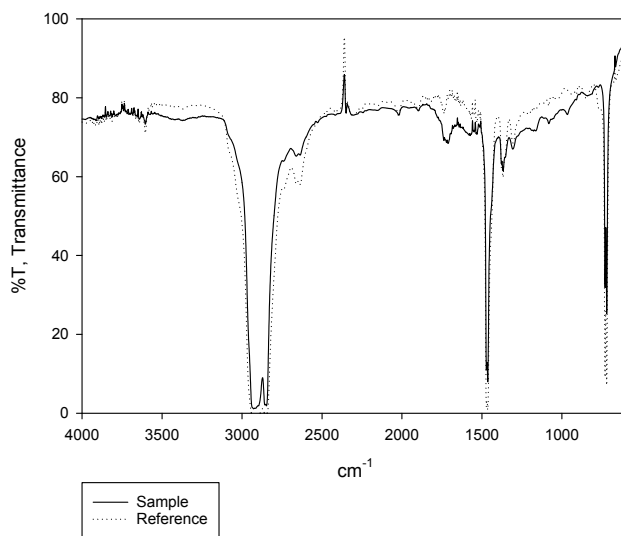

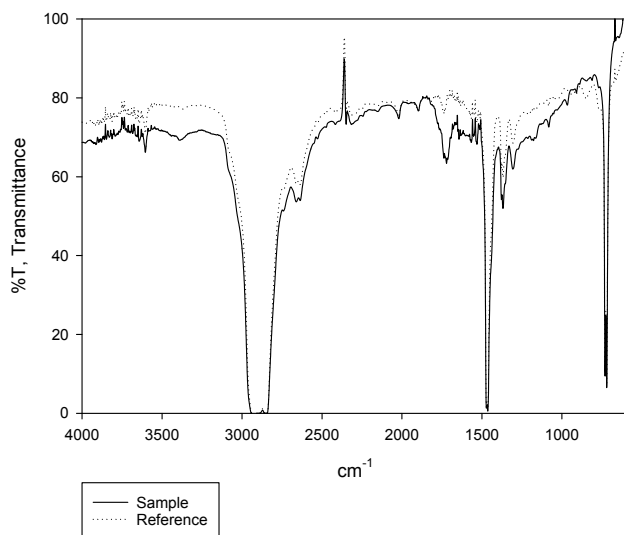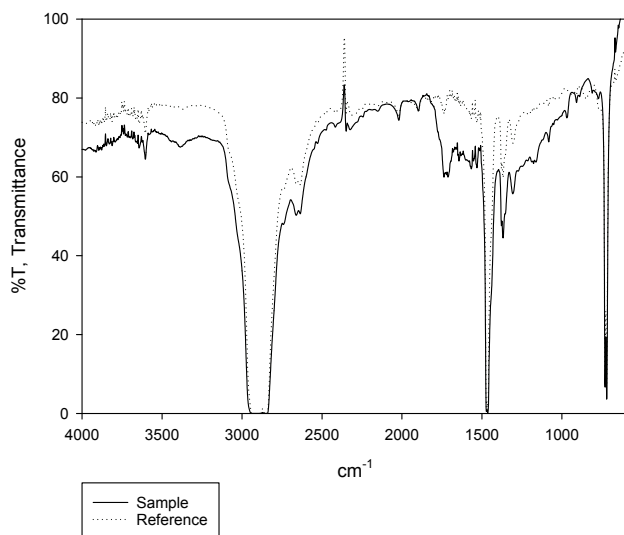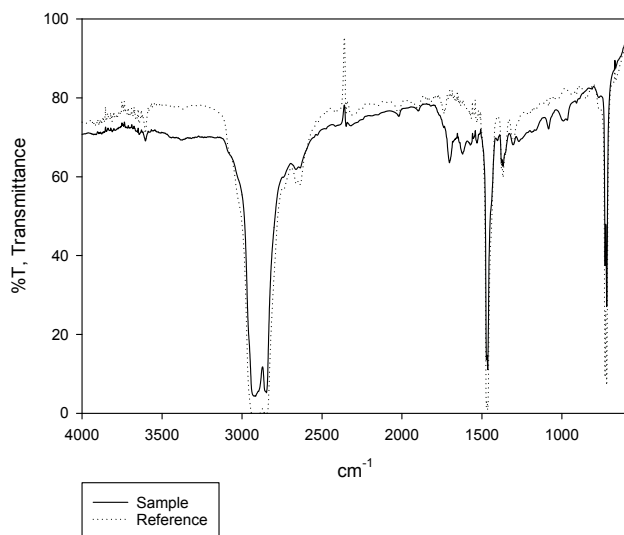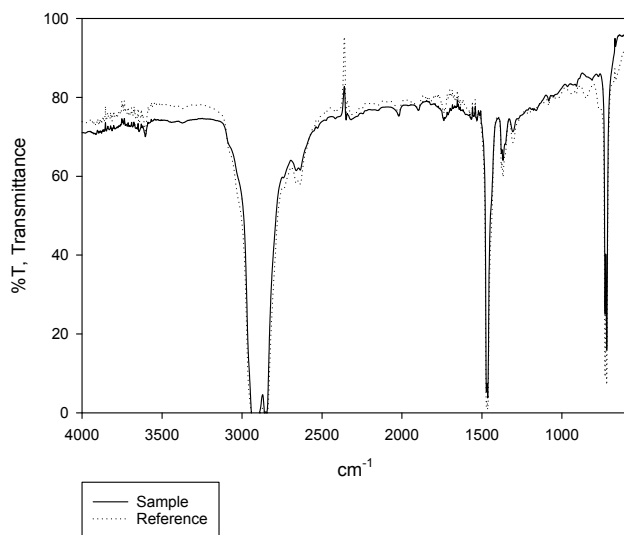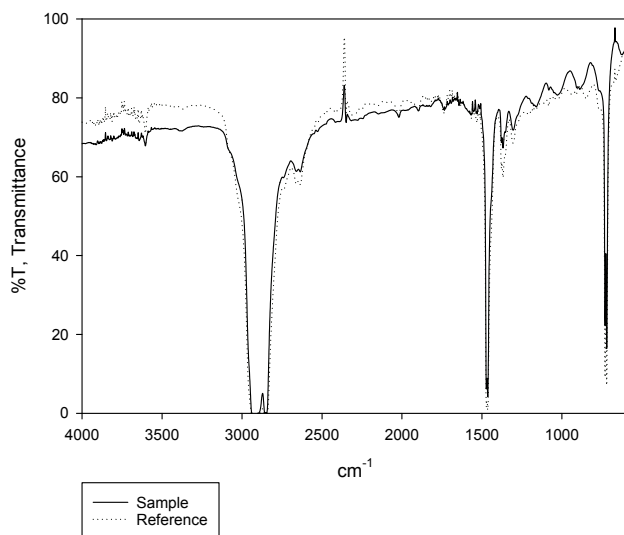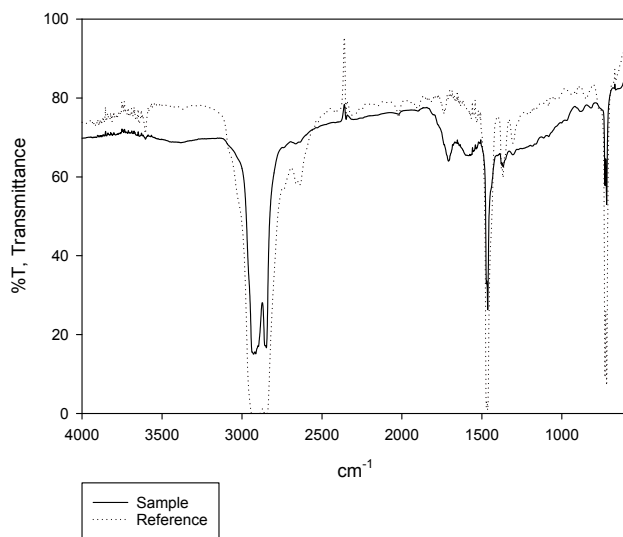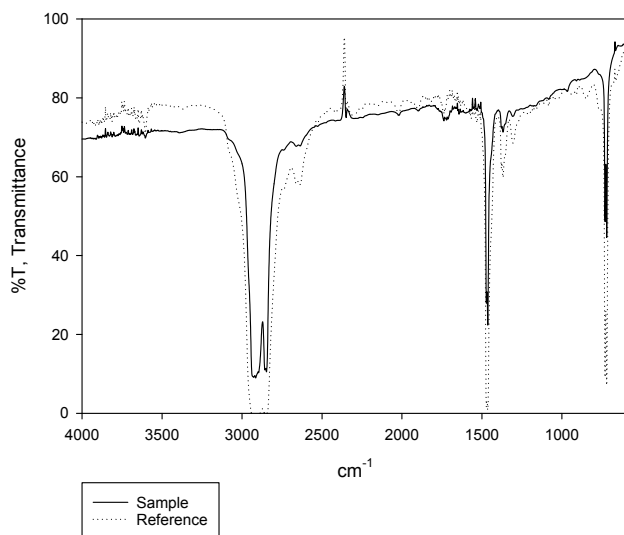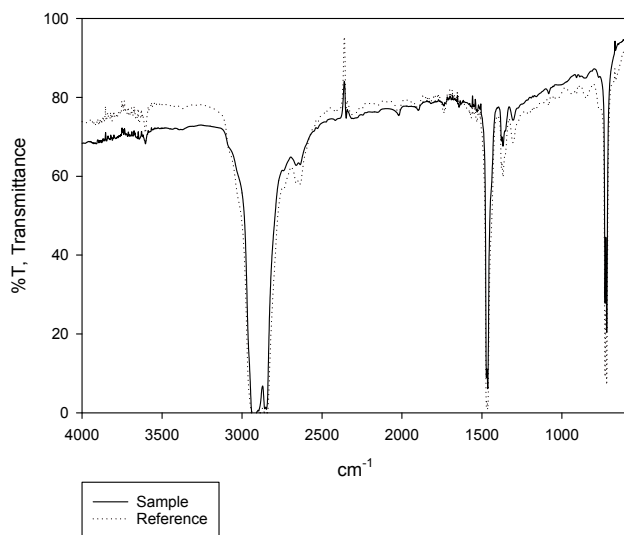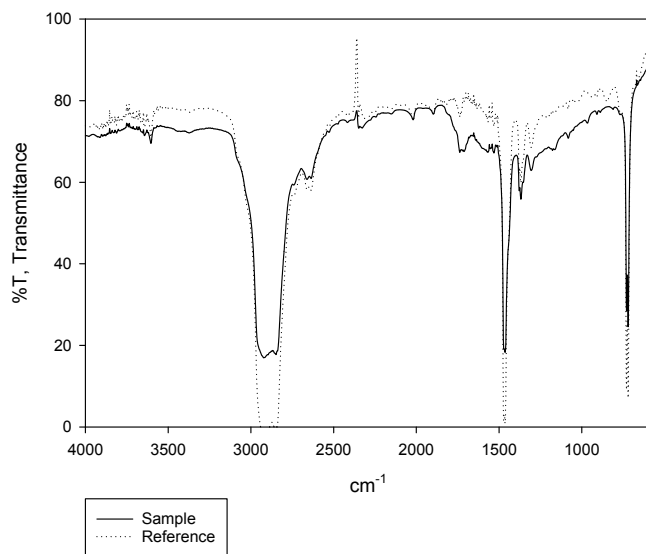**Figure A.2:** FT-IR spectrum of a category 1 contamination (third picture, second row in Figure B.2).

Figure A.3: FT-IR spectrum of a category 1 contamination (first picture, fourth row in Figure B.2).

A.2 Category 2

Figure A.4: FT-IR spectrum of a category 2 contamination (third picture, third row in Figure B.2).

Figure A.5: FT-IR spectrum of a category 2 contamination (first picture, fifth row in Figure B.2).

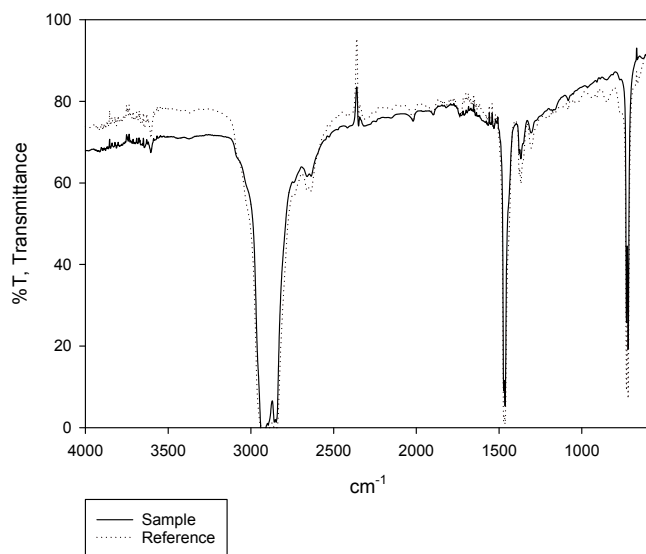**Figure A.6:** FT-IR spectrum of a category 2 contamination (third picture, fifth row in Figure B.2).

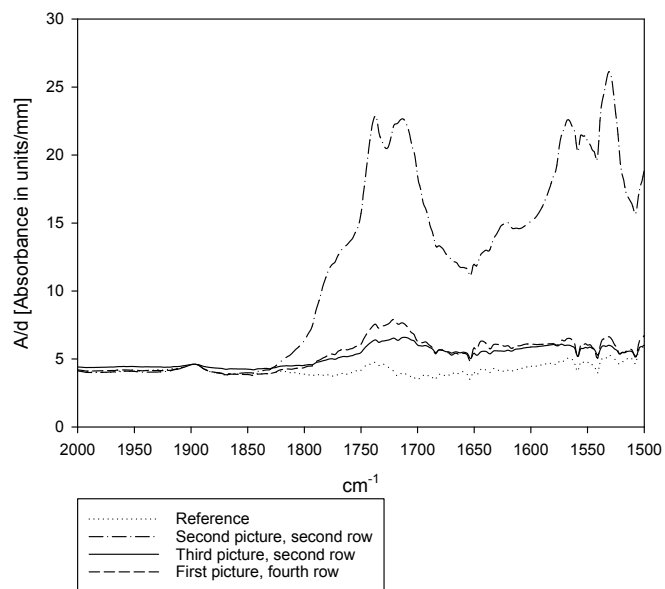**Figure A.7:** FT-IR spectrum of a category 2 contamination (second picture, third row in Figure B.2).

A.3   Category 3

Figure A.8: FT-IR spectrum of a category 3 contamination (second picture, fourth row in Figure B.2).

Figure A.9: FT-IR spectrum of a category 3 contamination (third picture, first row in Figure B.2).

Figure A.10: FT-IR spectrum of a category 3 contamination (first picture, second row in Figure B.2).

Figure A.11: FT-IR spectrum of a category 3 contamination (third picture, fourth row in Figure B.2).

Figure A.12: FT-IR spectrum of a category 3 contamination (second picture, fifth row in Figure B.2).

Figure A.13: FT-IR absorbance spectrum of category 1 contaminations, C=O region. The legend refers to the pictures in Figure B.2
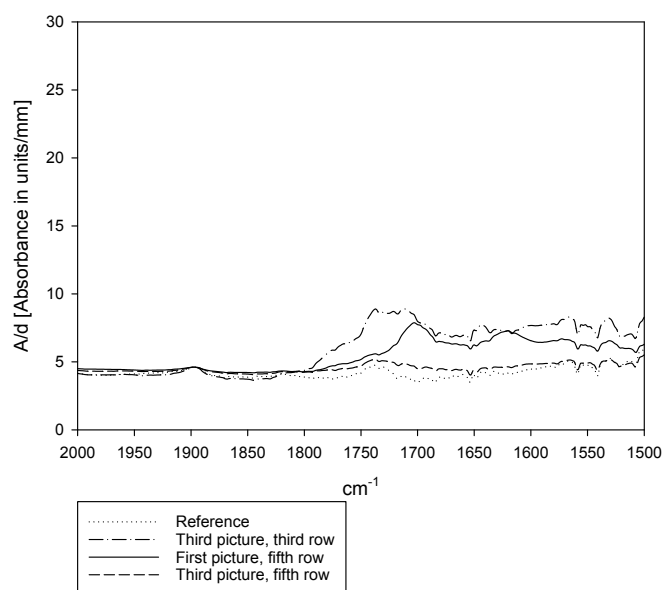

Figure A.14: FT-IR absorbance spectrum of category 2 contaminations, C=O region. The legend refers to the pictures in Figure B.2
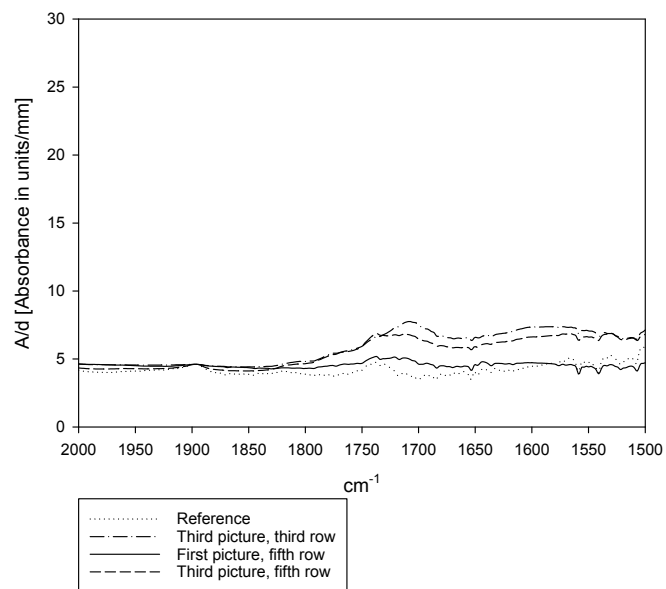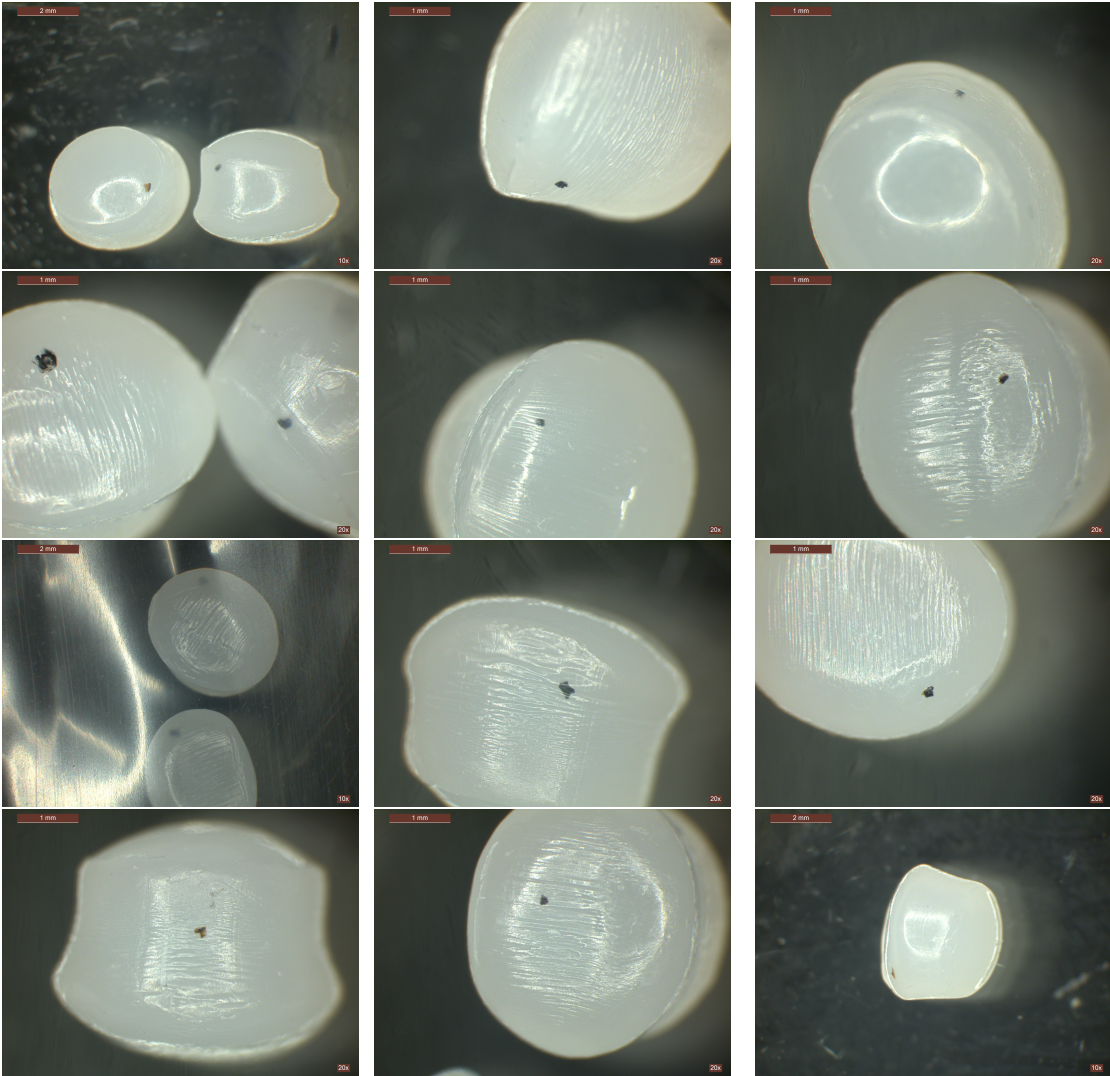
Figure A.15: FT-IR absorbance spectrum of category 3 contaminations, C=O region. The legend refers to the pictures in Figure B.2

B   Pellet Contaminations: Microscope Pictures

B.1   Whole Pellets

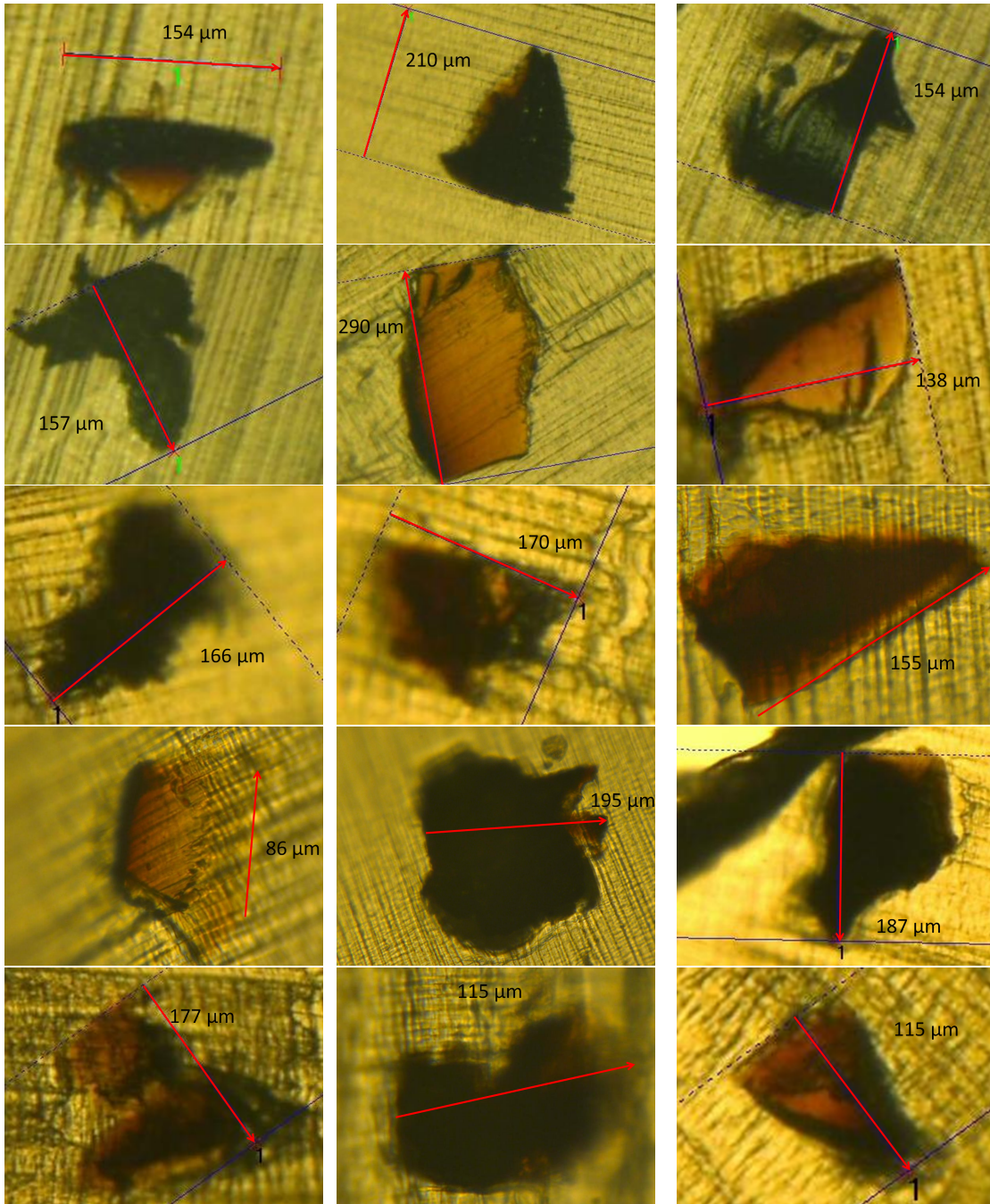## B.2   Mictromed Sections (∼25-30 μm thick)

Figure B.2: Microscope pictures of microtomed pellet contaminations.

C   Maxwell capacitors and interfaces at DC

If a DC voltage U is applied at time $t = 0$, the field E_a in the single Maxwell capacitor in Figure 2.3b can with Equation 2.9 be shown to be [6]:

$$E_a = \frac{\sigma_b U}{b\sigma_a + a\sigma_b}(1 - e^{-t/\tau}) + \frac{\epsilon_b U}{b\epsilon_a + a\epsilon_b}e^{-t/\tau} \tag{C.1}$$

where the time constant $\tau = \frac{b\epsilon_a + a\epsilon_b}{b\sigma_a + a\sigma_b}$, which has been shown to be up to 300 hours for HDPE [6]. From Equation C.1 it can be seen that the field E_a will tend towards a resistive field as t tends to infinity.

Surface charges will accumulate at interfaces between materials with different quotient ϵ/σ, such as in the case of charge layers, or a contaminant in cable insulation. The growth of these charges can be calculated with Gauss' law $\nabla\epsilon E = \rho$, and in the case of the interface in a single Maxwell capacitor this becomes

$$\epsilon_a E_a - \epsilon_b E_b = \kappa \tag{C.2}$$

where κ is the surface charge at the interface. Since $aE_a + bE_b = U$ and thus $E_b = \frac{U}{b} - \frac{a}{b}E_a$, it then follows that [6]

$$\kappa = U\frac{\sigma_b\epsilon_a - \sigma_a\epsilon_b}{b\sigma_a + a\sigma_b}(1 - e^{-t/\tau}) \tag{C.3}$$

It can be shown that the maximal attainable surface charge κ increases with the permittivity of the strongest insulator of the dielectrics. The maximal attainable surface charge is independent of the conductivity of the materials [6].

Equation C.3 can also be derived by calculating the DC field both capacitively and resistively in any configuration with an interface between two dielectrics. For both cases, the tangential field strengths will be equal at both sides of the interface:

$$E_{t1} = E_{t2} \tag{C.4}$$

which can be shown from $\nabla \times \vec{E} = 0$. Equation 2.9 in the static form ($\frac{\partial\rho}{\partial t} = 0$) can be written as $\nabla\vec{J} = 0$, from which it follows that

$$\sigma_1 E_{n1} = \sigma_2 E_{n2} \tag{C.5}$$

where E_{n1} and E_{n2} are the normal field strengths at both sides of the interface. Calculating the field capacitively implies using Equations C.2 and C.4, while calculating it resistively implies using Equations C.5 and C.4. Setting these sets as equal gives $\kappa = (\epsilon_1 - \epsilon_2\frac{\sigma_1}{\sigma_2})E_{n1}$ which is equivalent to equation C.3 in the case of a Maxwell capacitor. A resistively calculated field is thus a capacitively calculated field including the effect of the surface charge κ.

D   AC Breakdown Strength: Complete Table

Table D.1: AC step-up breakdown strengths kV_{rms}/mm as a function of days of DC pre-stress (31.5 kV/mm).

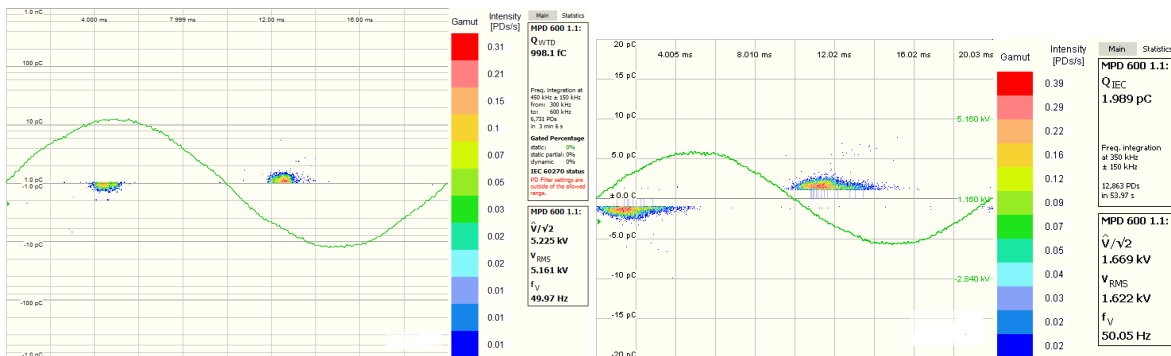| Object category	Days of prestress			
	0	9	35	163
A (without particles)	23.3	26.7	26.7	46.7
	30.0	33.3	26.7	60.0
	36.7	36.7	30.0	60.0
	40.0	40.0	33.3	66.7
	56.7	43.3	36.7	73.3
	56.7	46.7	40.0	73.3
B (with oxidized particles)	23.3	30.0	26.7	33.3
	26.7	30.0	33.3	60.0
	26.7	30.0	33.3	66.7
	30.0	30.0	40.0	66.7
	50.0	36.7	46.7	76.7
	53.3	36.7	46.7	76.7
C (with metal inclusions)	20.0	26.7	16.7	33.3
	26.7	26.7	26.7	33.3
	26.7	30.0	26.7	33.3
	30.0	33.3	30.0	40.0
	30.0	33.3	36.7	40.0
	40.0	36.7	36.7	40.0

E   Images of PD Activity Before and After DC Pre-stress

The figures below show PD activity of Rogowski-profiled test objects with a bottom thickness of 0.75 mm before and after a DC pre-stress of 35 days at 31.5 kV/mm. The y-axis is in pC, and the green sinus is the applied voltage. The discharge pattern is typical to that of air-filled cavities in solid dielectrics or surface discharges. The color of the discharge regions indicate the intensity of discarges. Blue indicates few discharges, red many discharges.
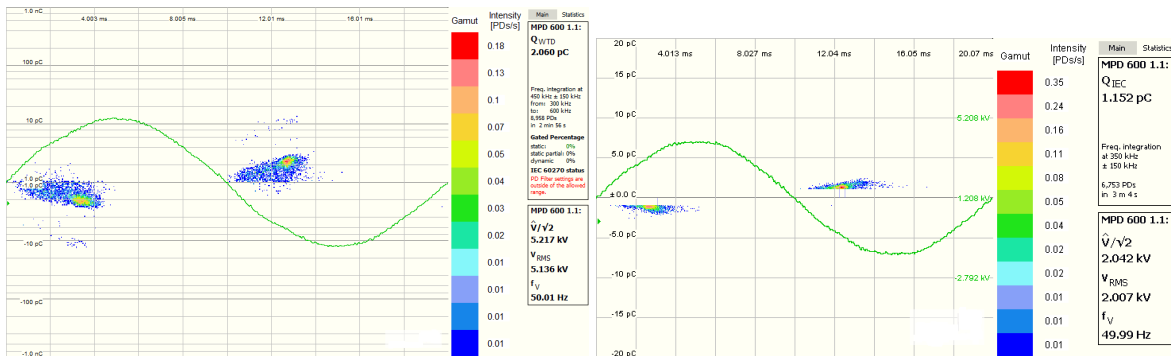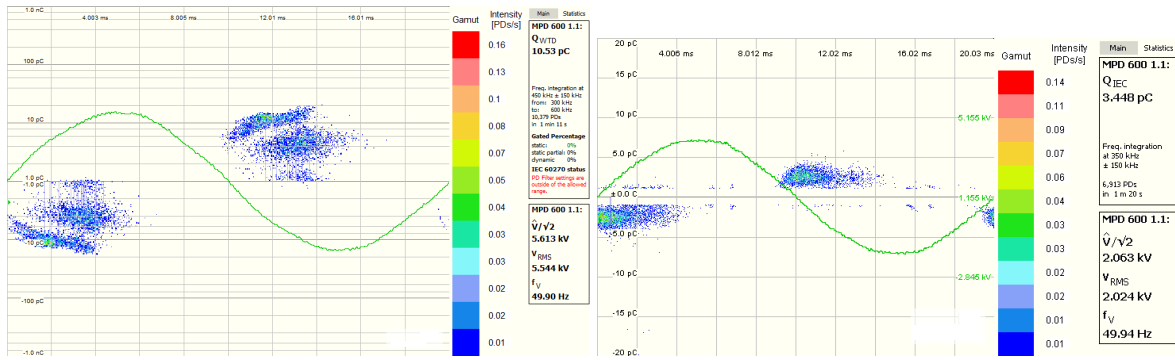

(a) Without DC pre-stress, inception at 5.1 kV. **(b)** With 35 days of DC pre-stress, inception at 2.0 kV.

Figure E.1: PD activity at inception voltage with and without DC pre-stress, of a category A object (A2 in Table 4.3).

(a) Without DC pre-stress, inception at 5.2 kV. **(b)** With 35 days of DC pre-stress. inception at 1.7 kV.

Figure E.2: PD activity at inception voltage with and without DC pre-stress, of a category B object (B2 in Table 4.3).

(a) Without DC pre-stress, inception at 5.5 kV.

(b) With 35 days of DC pre-stress, inception at 2.0 kV.

Figure E.3: PD activity at inception voltage, with and without DC pre-stress, of a category C object (C1 in Table 4.3).

F   Matlab Code: Normalization of Spectra

```
close all
Mref=dlmread('Referanse1_HKM.asc',' ',82,0)
M=dlmread('pellet3_HKM.asc',' ',82,0)

%convert to absorbance:

Aref=2-log10(Mref(:,2));
A=2-log10(M(:,2));

figure()
plot(Mref(:,1),Aref)
hold on

plot(Mref(:,1),A,'g')
hold on
%normalizing at 1897 Hz:

diff=A(4000-1896)/Aref(4000-1896)

Anorm=A/diff

plot(Mref(:,1),Anorm, 'r')

%returning to transmittance spectra

Tnorm=zeros(4001-580,1);
for i = 1:(4001-580)
Tnorm(i)=10^(2-Anorm(i));
end

%TO EXCEL
Data=[Mref(:,1) Mref(:,2) Tnorm Aref/0.025 Anorm/0.025]
filename= 'pellet3_HKM.xlsx';
xlswrite(filename, Data, 'A1:E3421')


hold off
plot(Mref(:,1),Mref(:,2))
hold on
plot(Mref(:,1),Tnorm,'r')
```